Structural Biology and Molecular Biophysics

Cryo-EM structures of Kv1.2 potassium channels, conducting and non-conducting

Reviewed Preprint

Revised by authors after peer review.

About eLife's process

Reviewed preprint version 2
May 28, 2024 (this version)

Reviewed preprint version 1
July 3, 2023

Posted to preprint server
June 3, 2023

Sent for peer review
May 22, 2023

Yangyu Wu, Yangyang Yan, Youshan Yang, Shumin Bian, Alberto Rivetta, Ken Allen, Fred J. Sigworth

Department of Cellular and Molecular Physiology, Yale University School of Medicine, New Haven, Connecticut USA

Abstract

Summary

We present near-atomic-resolution cryo-EM structures of the mammalian voltage-gated potassium channel Kv1.2 in open, C-type inactivated, toxin-blocked and sodium-bound states at 3.2 Å, 2.5 Å, 3.2 Å, and 2.9Å. These structures, all obtained at nominally zero membrane potential in detergent micelles, reveal distinct ion-occupancy patterns in the selectivity filter. The first two structures are very similar to those reported in the related Shaker channel and the much-studied Kv1.2-2.1 chimeric channel. On the other hand, two new structures show unexpected patterns of ion occupancy. First, the toxin α- Dendrotoxin, like Charybdotoxin, is seen to attach to the negatively-charged channel outer mouth, and a lysine residue penetrates into the selectivity filter, with the terminal amine coordinated by carbonyls, partially disrupting the outermost ion-binding site. In the remainder of the filter two densities of bound ions are observed, rather than three as observed with other toxin-blocked Kv channels. Second, a structure of Kv1.2 in Na^+ solution does not show collapse or destabilization of the selectivity filter, but instead shows an intact selectivity filter with ion density in each binding site. We also attempted to image the C-type inactivated Kv1.2 W366F channel in Na^+ solution, but the protein conformation was seen to be highly variable and only a low-resolution structure could be obtained. These findings present new insights into the stability of the selectivity filter and the mechanism of toxin block of this intensively studied, voltage-gated potassium channel.

eLife assessment

This **important** manuscript presents several structures of the Kv1.2 voltage-gated potassium channel, based on state-of-the-art cryoEM techniques and algorithms. The authors present **solid** evidence for structures of DTX-bound Kv1.2 and of Kv1.2 in potassium-free solution (with presumably sodium ions bound within the selectivity filter). These structures advance our knowledge of the molecular basis of the channel inactivation process.

https://doi.org/10.7554/eLife.89459.2.sa3

Introduction

Among the most-studied ion channel proteins is the Kv1 family of tetrameric, six- transmembrane-segment, voltage-gated potassium (Kv) channels. The best-known member of this family is the *Drosophila* Shaker channel, first cloned in the late 1980s (Iverson et al., 1988; Papazian et al., 1987) and which quickly became the favorite object for biophysical studies due to its small size and ease of heterologous expression. The potassium current in the squid giant axon described by Hodgkin and Huxley (Hodgkin & Huxley, 1952) is carried by a closely related Shaker homologue (Rosenthal & Bezanilla, 2002).

In 2005 Long et al. (2005) obtained the 2.9 Å crystal structure of Kv1.2, a mammalian Shaker-family channel. This structure showed clearly the overall architecture of the channel, but unfortunately the densities were weak in the all-important voltage-sensor domains (VSDs). Two years later Long et al. (Long et al., 2007) presented the 2.4Å X- ray structure of the "paddle chimera" Kv1.2-2.1 channel in which a portion of the voltage-sensor domain (the S3-S4 paddle) was replaced by the corresponding Kv2.1 sequence. This structure presented the VSDs in fine detail, and so was a watershed in the structural understanding of the many functional measurements of Shaker channels. It has also formed the basis of computational studies of voltage-sensing and gating mechanisms. A subsequent cryo-EM structure of Kv1.2-2.1 channels reconstituted into nanodiscs (Matthies et al., 2018) has excellent agreement with the X-ray structure.

Meanwhile, a very welcome recent development is the cryo-EM structure of the original Shaker channel itself (Tan et al., 2022).

The high-resolution structure of the Kv1.2 paddle chimera channel has been the basis for much research, but the native Kv1.2 channel has been used for more functional studies (Ishida et al., 2015; Suarez-Delgado et al., 2020; Wu et al., 2022). The properties of the native and chimeric channels are similar but not identical (Tao & MacKinnon, 2008). The chimeric channel has 27 amino-acid differences in the S3-S4 paddle region, but the VSD structures of Long et al. (2005 and 2007) are remarkablysimilar; in the transmembrane region the !-carbon traces are nearly superimposable. Our structure of Kv1.2 confirms this remarkable structural conservation.

Inactivation is an important process that diminishes voltage-gated channel current even when the activating membrane depolarization is maintained. A relatively slow inactivation process, usually called C-type inactivation (Hoshi et al., 1991) involves conformational changes in the pore domain and the selectivity filter. Various mutations in the pore domain have been shown to accelerate or impede C-type inactivation. The Shaker pore-domain mutation W434F renders the channel almost completely non- conductive through a process like C-type inactivation (Perozo et al., 1993; Pless et al., 2013; Suarez-Delgado et al., 2020; Yang et al., 1997). Structures of this mutant (Tan et al., 2022) and of a corresponding mutant Kv1.2-2.1 paddle-chimera channel (Reddi et al., 2022) show a dramatic dilation of the selectivity filter that disrupts two of the four ion-binding sites in the selectivity filter. We report here the structure of the corresponding W366F mutant in the Kv1.2 channel background, which shows a nearly identical dilation.

An important aspect of C-type inactivation is that it is enhanced when potassium ions are absent. In KcsA the replacement of most K^+ with Na^+ results in a collapse of the selectivity filter region, occluding the two central ion-binding sites (Zhou et al., 2001). Other channels including NaK2P and members of the K2P family show a destabilization of the external part of the pore at low K^+ concentrations, abolishing the two outer ion- binding sites (Lolicato et al., 2020; Matamoros et al., 2023; Sauer et al., 2011). In low potassium the NaK2P channel actually shows a dilation of the outer selectivity filter very similar to that seen in Shaker-W434F and the corresponding K1.2-

2.1 mutant. On the other hand, a lengthy molecular-dynamics simulation of deactivation in the Kv1.2-2.1 chimera channel in symmetrical K^+ solutions showed that, with the closing of the channel gate, there is a complete loss of water and ions from the cavity below the selectivity filter. Under these conditions however the selectivity filter remains intact and is populated by K^+ ions (Jensen et al., 2012); M. Ø. Jensen, personal communication).

In view of the variety of effects of low K^+, in our current study we sought to observe experimentally the structure of the Kv1.2 channel when potassium ions are absent.

Finally, Kv channels are targets for many toxins that inhibit channel conductance, with a common mechanism being occlusion of the pore. This occlusion has been seen directly in two cases. Crystal structures of the Kv1.2 paddle-chimera channel have been obtained with charybdotoxin (CTx) bound (Banerjee et al., 2013), and cryo-EM structures of Kv1.3 with the ShK toxin bound (Selvakumar et al. 2022). In the present work we consider dendrotoxins (DTxs) produced by the mamba snake *Delodiaspis*.

These are distinct from CTx but also block Kv channels with high potency and selectivity (Gasparini et al., 1998). In this study we have determined the structure of Kv1.2 with α- DTX bound.

Results

Overview of mammalian Kv1.2 structure

For this study we employed a full-length Kv1.2 α-subunit construct containing three mutations in disordered regions of the N-terminus and S1-S2 linker. We denote this construct used for structure determination Kv1.2s. We co-expressed a construct of of Kvβ2 (Gulbis et al., 1999) containing residues 36 to 367. Each β2-subunit contained five mutations chosen to neutralize positive charges on the cytoplasmic face of the subunit; these remove strong, interfering interactions with cryo-EM carbon substrates. We find that the mutations have no effect on β-subunit secondary structure. Although α and β subunits were co-expressed, in cryo-EM micrographs we observed many α4 complexes along with the expected α4β4 particles. As the structures of the transmembrane regions of these two populations of channels were indistinguishable, we combined the two particle sets. This is reasonable as the presence of β2 subunits has very little effect on the structure of the α-subunit T1 domains to which they bind (Gulbis et al., 2000) and also little effect on channel function (Rettig et al., 1994).

The constructs encoding the Kv1.2s or Kv1.2s-W366F mutant α-subunits, along with the β2 subunits, were expressed in *Pichia pastoris* essentially as described (Long et al., 2005). Channel complexes were affinity-purified in the presence of dodecylmaltoside detergent and subjected to size-exclusion chromatography in buffers containing either 150 mM K^+ or 150 mM Na^+ ions. The channel complexes were plunge-frozen on grids for cryo-EM analysis. Focusing on the transmembrane region of the Kv1.2 channel complexes, we obtained structures of nominally open, C-type inactivated, DTx-bound, and K^+ free states at resolutions of 3.2 Å, 2.5 Å, 3.2 Å and 2.9 Å respectively. Most main-chain and sidechain densities were clearly visible in the resulting maps allowing atomic models to be built with high confidence.

Structures of the Kv1.2s channel (**Figure 1A-C**, and **Figure 1—figure supplement 1**) are very similar to those of the Kv1.2-2.1 chimera (Long et al., 2007) and *Drosophila* Shaker (Tan et al., 2022) channels. As observed in other Kv1 and Kv2 structures, the voltage- sensing domains (VSDs) contain the membrane-spanning S1-S4 helixes (**Figure 1D and E**) while the S5, S6, pore

helix and selectivity filter P-loop form the ion-conduction pore in a domain-swapped configuration. Densities of lipids bound to the VSDs and pore domains (PDs) are clearly visible in the Kv1.2s maps (**Figure 1A**).

In the critical region of the voltage-sensor domain (VSD) the sidechains of the voltage- sensing Arg and the coordinating Glu and Asp residues, as well as the charge-transfer center phenylalanine (Tao et al., 2010) are essentially superimposable with Shaker (**Figure 1D**), with an RMS difference of all Arg sidechain atoms of 0.85 Å. As Kv1.2 is a member of the Shaker potassium channel family and has 68% amino-acid identity with *Drosophila* Shaker, it is not surprising that the fold is very similar.

As in the other homologues an open S6 gate is visible in the detergent-solubilized Kv1.2s structure; this is expected for the open conformation at zero membrane potential.

Seeing no evidence of a barrier to ion flux, we call this the open-channel structure (**Figure 2B**).

Despite the very closely matched open-state structures of the VSDs it is therefore puzzling that the total gating charge movement in Shaker channels is larger, about 13 elementary charges per channel, while it is only 10 e0 per channel in Kv1.2 (Islas, 2016). The most likely explanation is that in Kv1.2 there is some additional restraint, lacking in Shaker, on the physical displacement of each S4 helix.

In the paddle chimera a region including the N-terminal half of the S4 helix in Kv1.2 is replaced by the corresponding Kv2.1 sequence. One difference in the voltage-sensing residues is that a glutamine replaces the arginine at the first position (R1) in the chimera. Another difference is that there is an earlier Arg residue R0 that replaces leucine, but is unlikely to contribute to charge movement. A direct measurement of charge movement in the paddle chimera is lacking, but macroscopic activation and inactivation show lower voltage sensitivity (Tao & MacKinnon, 2008) as if its gating charge movement were reduced. Nevertheless, as was observed by Long et al. (2007), the structures of the S4 regions are very similar: comparing Kv1.2 with the paddle chimera (**Figure 1E**) the rms deviation of Arg sidechain atoms is less than 0.75 Å.

Channel inactivation

Figure 2 compares the structure of the open channel with that of the Kv1.2s-W366F mutant. While the corresponding mutation W434F in Shaker essentially abolishes ion current through the channel (Yang et al., 1997) the Kv1.2s mutant allows currents to flow transiently on depolarization, but decay to less than 3% of the peak within 80 ms (**Figure 2—figure supplement 1**). Inactivation in these channels can be slowed by raising extracellular K^+ or by applying tetraethylammonium ion (Suarez-Delgado et al., 2020), properties that are hallmarks of C-type inactivation. Here we shall call the cryo-EM structure of Kv1.2s-W366F the “inactivated channel” structure, keeping in mind that other distinct inactivated channel conformations are likely to exist. The overall conformational difference between open and inactivated structures in Kv1.2s is identical to the difference observed in structures of Shaker (Tan et al., 2022) and in structures of Kv1.2-2.1 (Long et al. 2007; Reddi et al., 2022).

For detailed comparison with structures of other voltage-gated potassium channels, we borrow from Miller (1990) the numbering of the 39 residues in the S5-S6 linking region, which we will denote as residue numbers 1’ to 39’. (**Figure 2A**). The 39-residue numbering is appropriate for Kv1 through Kv4 channels (Shealy et al., 2003) and is fortuitously convenient in comparisons with KcsA, because it differs numerically by exactly 50 from the residue numbering of KcsA. In the Miller system for example the Kv1.2 W366 residue is W17’, and we can denote the W366F mutant channel as Kv1.2s- W17’F. In KcsA the W17’ residue is W67.

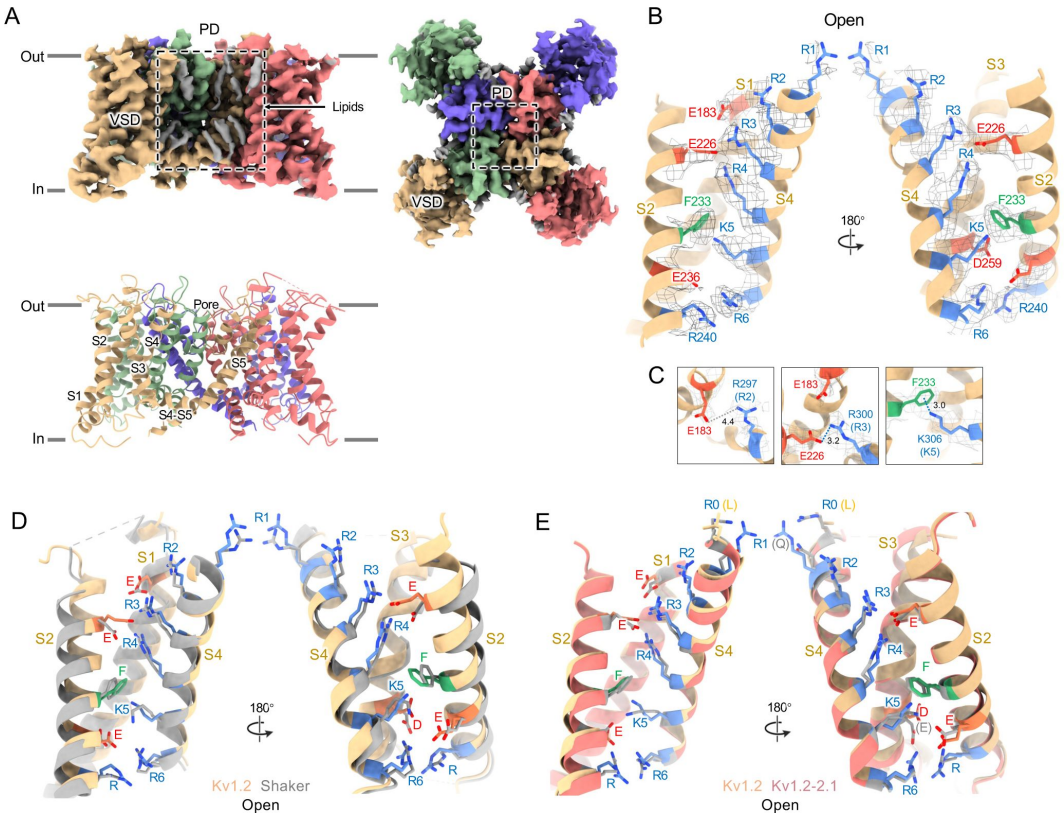

Figure 1.

Open Kv1.2 overall structure.

(A) Side and top view of the Kv1.2s cryo-EM density map (upper panel) and model (lower panel). Lipid densities are colored gray in the map. (B) Side view of VSD structure with map density of Kv1.2$_S$. (C) The relative positions of the interacting residues R2 and E138 (upper), R3 and E226 (middle), K5 and F233 (lower) are shown. (D) Superposition showing the very close match of Kv1.2 (yellow) and Shaker (gray) VSD structures. (E) Superposition of Kv1.2s (yellow) and Kv1.2-2.1 (pink) VSD structures. Positively charged, negatively charged and aromatic residues are shown as blue, red and green, respectively. VSD, voltage-sensing domain; PD, Pore domain.

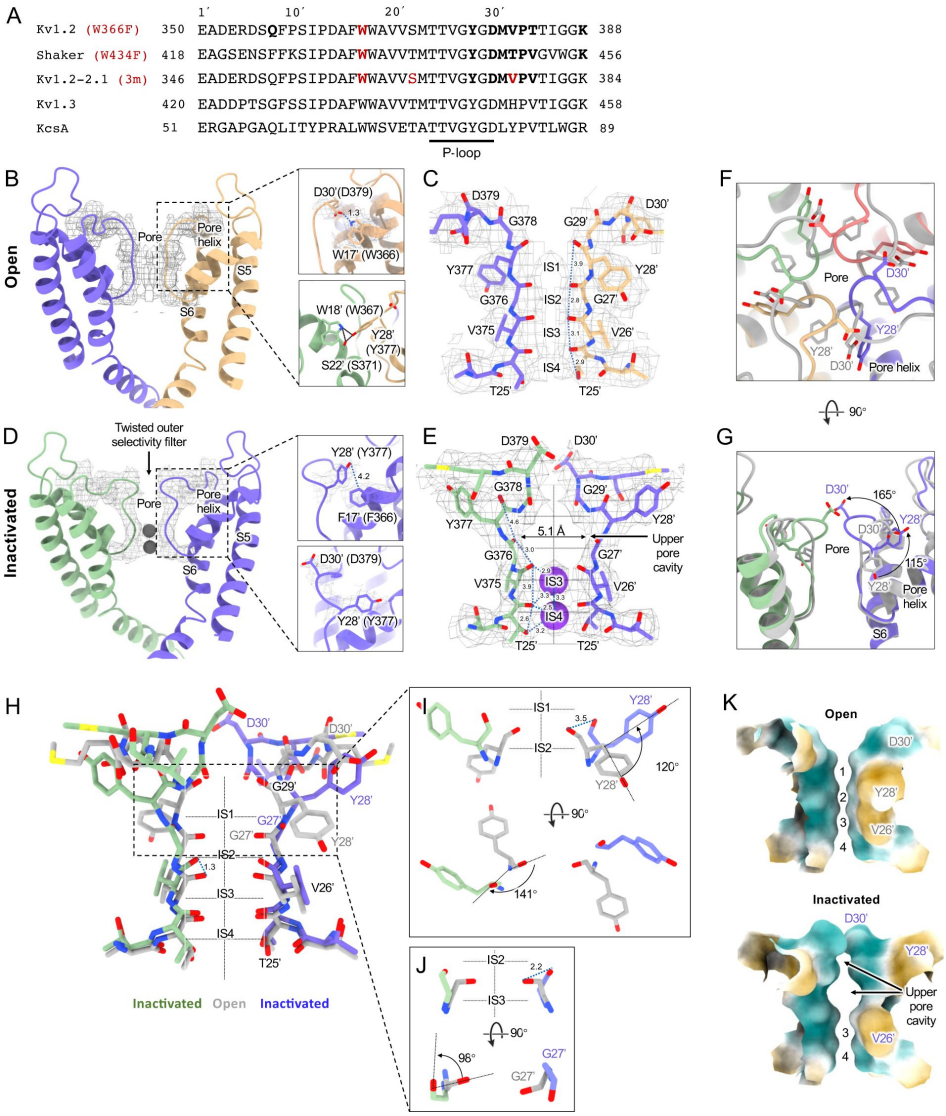

Figure 2.

Kv1.2 pore domain and selectivity filter structures in inactivated and open conformations. (A) Sequence alignment of potassium channels in the S5-S6 linker region, with the relative numbering of Miller (1990) indicated at top. (B) Side view of opposing subunits in the open Kv1.2s pore domain. Relative positions of Y28′, W17′ and D30′ are shown in the right- hand panels. Shown with a dashed blue line is the key hydrogen bond between D30′ and W17′ that is eliminated in the W17′F (W366F) mutant. (C) Side view of opposing Kv1.2s P-loops. Labels on the left show the Kv1.2 residue numbering, and on the right the Miller numbering. (D) Side view of the inactivated Kv1.2s W17′F pore domain. The new locations of Y28′, F17′ and D30′ are shown in the right panels. (E) Side view of the Kv1.2s P-loop in the inactivated conformation. In the large upper-pore cavity the G27′ and G29′ carbonyls are 5.1 and 11 Å apart. Potassium ions are shown as purple balls. (F) Superimposed top views of the Kv1.2s outer pore in inactivated (colored) and open (grey) states. In the inactivated channel the displaced Y28′ ring of one subunit is in the position occupied by D30′ - in the neighboring subunit - of the open channel. (G) The corresponding side view. The large rotation of the Y28′ side chain and flipping of D30′ are indicated by curved arrows. (H) Side view of the P-loop in inactivated (colored) and open (grey) conformations. (I,J) Details of Y28′ G27′ carbonyl and side chain reorientation from open (grey) to inactivated (colored) states are shown in side view (upper) and top view. (K) Surface renderings of open and inactivated selectivity filter region. Hydrophilic and hydrophobic surfaces are shown in teal and orange, respectively.

The selectivity filter of potassium channels consists of an array of four copies of the extended loop (the P-loop) formed by a highly conserved sequence, in this case TTVGYGD. The main-chain carbonyl oxygens of the residues TVGY, positions 25' to 28', delineate ion binding sites S3, S2 and S1, respectively, while the lower (most intracellular) edge of binding-site S4 is formed by the T25' hydroxyl. Hydrogen bonds involving two P-loop residues anchor the outer half of the selectivity filter and are particularly important in inactivation mechanisms (**Figure 2B**, right panels) (Pless et al., 2013; Sauer et al., 2011). Normally, the tyrosine Y28' (Y377 in Kv1.2) is constrained by hydrogen bonds to residues in the pore helix and helix S6 and is key to the conformation of the selectivity filter. The final aspartate of the P-loop, D30' (D379 in Kv1.2) is normally located near the extracellular surface and has a side chain that also participates in H-bonds with W17' (W366 in Kv1.2) on the pore helix.

The difference between the open and inactivated Kv1.2s structures, like the open- inactivated state differences in Kv1.2-2.1 (Reddi et al., 2022) and in Shaker (Tan et al., 2022) can be imagined as resulting from a two-step process. The first step is a partial twist of the P-loop backbone involving D30'. When W17' is mutated to phenylalanine, it is no longer an H-bond donor to D30' (**Figure 2D** right upper panel). The resulting destabilization of D30' allows it to reorient toward the external water-filled vestibule.

The second step is the reorientation of Y28' and further twisting of the polypeptide backbone. Y28' normally participates in H-bonds with the pore-helix residues W18' and S22' (**Figure 2D** right lower panel), but with the release of D30', and presumably the entry of water molecules into the space surrounding the P-loop, the side chain of Y28' also reorients toward the external solution, filling some of the original volume occupied by the side chain of D30'. The reorientation of the phenol group of Y28' is through a very large pitch angle of about 120° (**Figure 2G,H**,I). The reorientations of the D30' and Y28' side chains drag and twist the backbone. The result is an enlargement of the ion- binding site IS2 to a width of 5.1Å between opposing carbonyl oxygens (**Figure 2E**) and an even wider (11 Å) cavity is formed at the level of IS1. There are no clear ion densities in the upper selectivity filter.

Meanwhile, the lower binding sites IS3 and IS4 show relatively small disturbances in the inactivated state. The largest change is a rise of 1.3Å in the position of the G27' carbonyl, the one which defines the top of IS3 (**Figure 2J**). As in the inactivated Shaker structure (Tan et al., 2022) strong ion densities are seen in IS3 and IS4.

Might symmetry-breaking accompany Kv1.2 inactivation? MD simulations of inactivated paddle chimera, KcsA and hERG channels (Kondo et al., 2018; Li, Shen, Reddy, et al., 2021; Li, Shen, Rohaim, et al., 2021), all homotetramers, show a change to two-fold symmetry in the pore region such that the selectivity filter has distinct conformations for each pair of opposing subunits. However, we were not able to detect any evidence of reduced symmetry in the inactivated Kv1.2 channel. We were able to build the atomic model unambiguously into the 2.5 Å map that was obtained with C4 symmetry imposed. Further, there was no evidence of broken symmetry when using symmetry expansion and local C1 refinements of the cryo-EM dataset.

A comparison of our open-channel and inactivated Kv1.2s structures show subtle but noticeable differences in the VSDs. Salt bridges involving the S4 Arg and Lys residues are shifted slightly (**Figure 2—figure supplement 3A-D**). Arg300 (R3) is in close proximity to Glu226 on the S2 helix for the open channel, while R3 is closer to Glu183 in the S2 helix. The Glu226 side chain adopts a visible interaction with R4 in the inactivated state. In both open and inactivated states of Kv1.2s, K5 interacts more closely with S2 Phe233 than is the case in the paddle chimera channel (**Figure 1E**).

Functional interactions have been observed between residues in the voltage-sensing domains and pore residues involved in C-type inactivation (Bassetto et al., 2021; Conti et al., 2016). Leucine and valine residues on the S4 helix interface with serine and leucine residues on S5, which in turn contact F16' and W17' on the pore helix. We see very little relative movement of the residues at the S4-S5 interface, much less than 1Å difference between open and inactivated structures.

While the VSD helices in Kv1.2s and the inactivated Kv1.2s-W17'F superimpose very well at the top (including the S4-S5 interface described above), there is a general twist of the helix bundle that yields an overall rotation of about 3° at the bottom of the VSD. In moving to the inactivated state, the axes of the helices S0, S1 and S2 tilt by 6°, 4° and 3.2° in a clockwise direction as viewed from the cytoplasmic side, while S4 is stationary. This lower VSD rotation provides a good explanation of the shifts in the S2 residues Glu183 and Glu226 that interact with R2 and R3 (**Figure 2—figure supplement 3E-F**). In contrast to Kv1.2s, neither Shaker and Kv1.2-2.1 structures show this rotation between open and inactivated states (**Figure 2—figure supplement 3G-H**) but instead the VSDs remain superimposable.

It should be noted that the difference between Kv1.2s and the others in conformational changes might arise from the variety of systems used for structure determination, which include DDM micelles, MSP-bounded nanodiscs, and crystals grown in different laboratories (but under very similar conditions and having the same space group). In the Kv1.2s case for example, the detergent micelles might allow the VSDs to be particularly mobile.

A dendrotoxin blocks Kv1.2 by inserting a lysine into the pore

Dendrotoxins are peptide neurotoxins from mamba snakes that bind with nanomolar affinities and block potassium channels. Alpha-dendrotoxin (α-DTX) consists of a peptide chain of 59 amino acids stabilized by three disulfide bridges (**Fig. 3A**) and, like other dendrotoxins, exhibits the same fold as Kunitz protease inhibitors (Skarzynski, 1992). In α-DTX arginine and lysine residues are concentrated near the N-terminus (Arg3, Arg4, Lys5), the C-terminus (Arg54, Arg55) and at the narrow β-turn region (Lys28, Lys29, Lys30). The Lys5 side chain protrudes from the surface of the molecule, and its modification by acetylation markedly reduces binding (Harvey et al., 1997).

Replacement of Lys5 by alanine or ornithine decreased the affinity for potassium channels by 1000-fold and 100-fold, respectively, suggesting that the sidechain geometry is critical (Gasparini et al., 1998). The Lys5 sidechain therefore has been the prime candidate for the pore-blocking residue. The nearby Leu9 is also important as its substitution by alanine also decreases affinity 1000-fold, but we observe no contacts between this residue and residues of the Kv1.2s channel.

By adding an excess of α-DTx to detergent-solubilized Kv1.2 protein we obtained a dataset of about 300,000 particles where an additional cap of density can be seen outside the pore (**Figure 3B**). In 3D classification only a small fraction (<1%) of toxin-free particles was detected, and this class was removed before further processing. The processing of particle images is summarized in **Figure 3** – figure supplement 1. Refined structures with imposition of four-fold symmetry (C4) or with no symmetry (C1), yielded resolutions 2.8 and 3.2 Å respectively. In the C4 reconstruction the additional cap of density from the toxin was not interpretable, as it arises from the four-fold superposition of the asymmetric toxin bound in alternative poses to the symmetric channel. Zhang et al. (Zhang et al., 2021) have demonstrated however that small asymmetric ligands can be distinguished in large single-particle datasets by focused classification and refinement. Similarly we used symmetry expansion, a reference mask covering only the toxin and upper selectivity filter, and a set of four asymmetric starting references to obtain, through 3D classification without alignment in the Relion software, a C1 reconstruction. The refined C1 density map and model are illustrated in **Figure 3**.

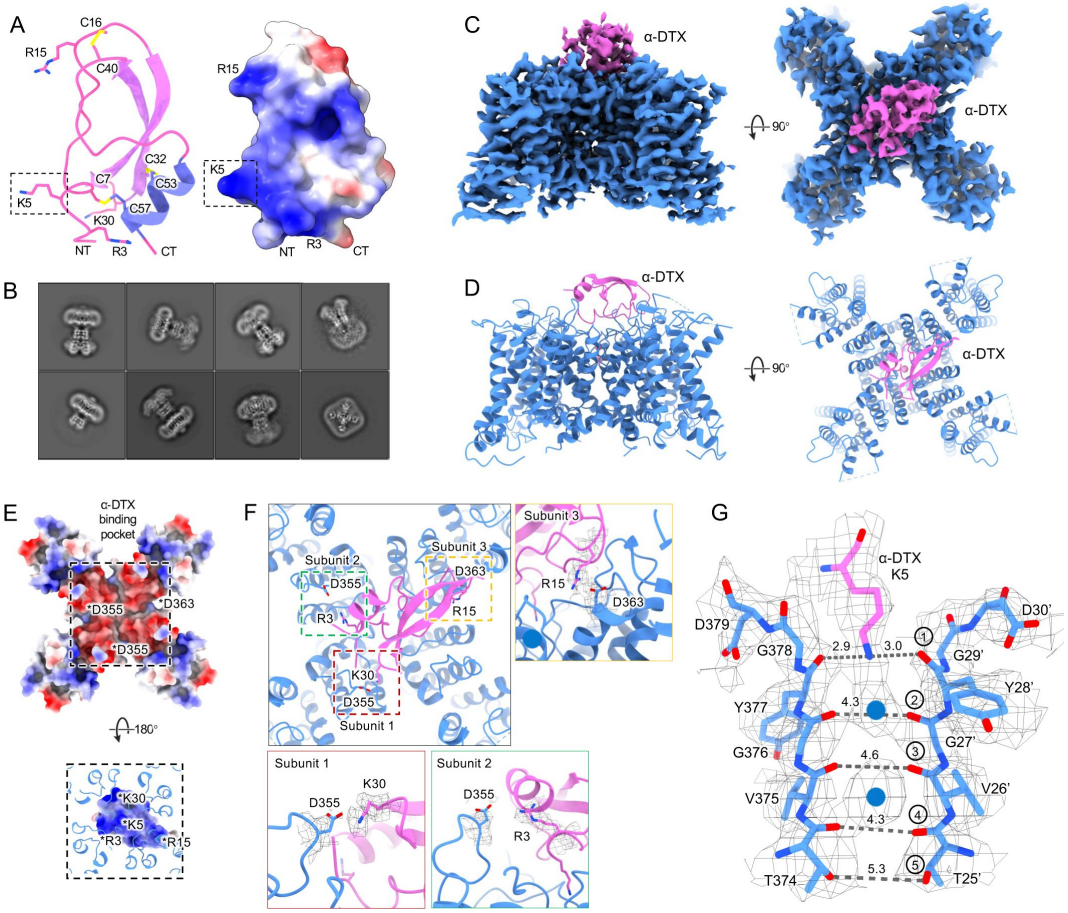

Figure 3.

Kv1.2s DTx-bound structure.

(A) DTx crystal structure (pdb:1DTX) and electrostatic surface view. Basic residue sidechains are illustrated, and disulfide bridges are shown in yellow. (B) Representative 2D classes from the DTx-bound Kv1.2s. (C) Side and top view of Kv1.2s-DTx cryo-EM density map, obtained with no symmetry imposed. (D) Side and top view of the fitted model. (E) Top-down view of the Kv1.2s-DTx structure with DTx removed, shown as electrostatic surface view (upper panel); the corresponding bottom-up view through the DTx-channel interface. DTx is shown in electrostatic surface view, and extensions of Kv1.2s helices in blue. The asterisks indicate the charged groups. (F) Three salt-bridge interactions between DTX and Kv1.2s are shown as top view (upper left panel) and side views. (G) Side view of the selectivity filter of Kv1.2s-DTx. Gray dashed lines show approximate distances between carbonyl oxygens. Potassium ions are shown as blue balls.

The X-ray structure of α-DTX (**Figure 3A**) could be docked with minor adjustments into the map, with the Lys5 sidechain extending into the channel pore. The positively- charged toxin is tethered to the negatively-charged outer mouth of the pore by three salt bridges: toxin residues K30, R15 and R3 bind to three channel residues D355, D363 and D363 (D6', D14' and D14' in the turret and pore helix). Each of the three channel residues is located on a different subunit (**Fig. 3E,F**).

In the selectivity filter of the toxin-bound channel (**Figure 3G**) a continuous density is seen to extend downward from the toxin to the boundary of IS1. This density is well modeled by the side chain of Lys5, with the terminal amine coordinated by the carbonyls of Y377 (Y28'). We conclude that block by α-DTx is occlusion of the selectivity filter through binding of the Lys5 terminal amine. In the selectivity filter a large density peak, presumably a K^+ ion, is seen in a somewhat offset IS1 binding site; a second, larger K^+ ion peak is seen in IS3.

We also tried mixing an excess of α-DTX with the Kv1.2s W366F protein sample in an attempt to observe a pore-blocker-bound inactivated structure. However, we found no evidence of bound toxin density on the channel in the cryo-EM 2D classes. This is no surprise in view of the large rearrangement of the extracellular pore entrance in the inactivated state, where the IS1 and IS2 sites are abolished and the corresponding carbonyls point away from the pore axis (**Figure 2E**), eliminating the site of binding of the lysine side chain. It should be noted however that in the case of a ShK toxin derivative binding to the Kv1.3 channel, Tyagi et al. (2022) observed that binding occurs to inactivated channels. In that case the inactivated state has a less drastically remodeled selectivity filter, and binding of the toxin restores the selectivity filter to its conducting configuration (Tyagi et al., 2022).

The Kv1.2 selectivity filter in K^+-free medium

The X-ray crystal structure of the KcsA channel in low K^+ solution (Zhou et al., 2001) shows a collapsed selectivity filter, in which the residues V26' and G27' are rearranged, abolishing the binding sites IS2 and IS3. In low K^+ other channels including KirBac2.2 and K2p10.1 show large conformational fluctuations of the outer pore in low K+ (Matamoros et al., 2023; Wang et al., 2019), and in the model potassium channel NaK2K the outer half of the selectivity filter unravels at low K^+ (Sauer et al., 2011). On the other hand, Shaker channels are seen to conduct Na^+ in the absence of K^+ (Melishchuk et al., 1998). Thus it is of interest to observe the structure of Kv1.2 under this condition.

We obtained the structure of Kv1.2s in a zero K^+ solution, with all potassium replaced with sodium, and were surprised to find that it is little changed from the K^+ bound structure, with an essentially identical selectivity filter conformation (**Figure 4B** and **Figure 4—figure supplement 1**). The ion occupancy is also similar, and we presume that Kv1.2 is a conducting channel in sodium solution. Like Kv1.2s in the usual potassium solution, the major Na^+ ion densities are seen in the IS1 and IS3 ion binding sites, with somewhat lower occupancy of IS2 and IS4 (**Figure 4B and E**). The increased asymmetry in ion occupancy is expected to reduce ion conductance. Such a situation was observed in the KcsA channel by Morais-Cabral et al. (2001) where densities of the less-permeant Rb^+ ions were observed also to be asymmetrically positioned in IS2 and IS4.

Large conformational fluctuations of the W366F mutant in K^+-free medium

We also collected cryo-EM data from the Kv1.2sW17'F mutant channels with Na^+ replacing K^+ in the final size-exclusion chromatography step. The corresponding Shaker-W17'F channel stably carries large Na^+ and Li^+ currents in the absence of K^+ (Starkus et al., 1998). In 2D classification of our single-particle images we saw large variability in the structure, as if the connection between

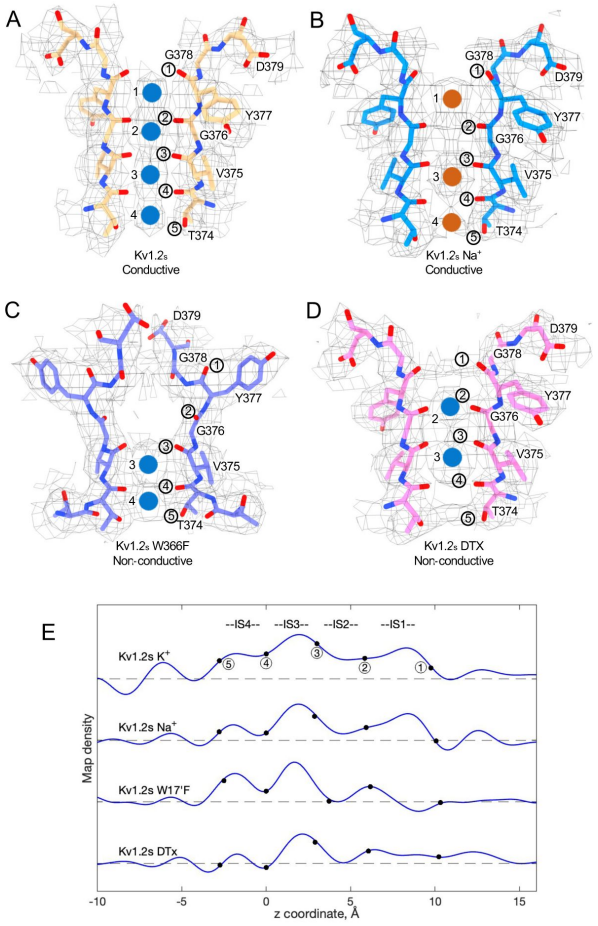

Figure. 4

Summary of Kv1.2 conductive and non-conductive pores. Selectivity filter structures of (A) Kv1.2s, (B) Kv1.2s Na+-bound, (C) Kv1.2s W366F, and (D) Kv1.2s-DTX. Potassium ions and sodium ions are shown as blue and orange balls, respectively. Circled numbers label the P-loop ion- coordinating oxygens. (E) Plots of density along the symmetry axis of the selectivity filter region. Values of the z-coordinate are relative to the position of the T25′ (T374) carbonyl oxygen. The nominal positions of the coordinating oxygens are marked and numbered as in parts A-D. Dashed baselines indicate the external solvent density. The scaling of the density traces is arbitrary. The DTx map was computed with no symmetry imposed; for the others, C4 symmetry was imposed in reconstruction.

the transmembrane domain and the intracellular domains (the T1 domain and the Kvβ2 subunits) was highly flexible (**Figure 5A-B**). The intracellular domains were resolved to 3.0 Å resolution in a focused reconstruction (**Figure 5C**) but the complementary focused reconstruction of the transmembrane domain yielded only about 7 Å resolution. Nevertheless this low- resolution map matches the secondary structure of the Kv1.2 W366F mutant in K^+ solution (**Figure 5D**), with the possible exception of low density in the selectivity filter region (**Figure 5E-F**). We conclude that the structure of this mutant channel becomes unstable in the absence of K^+, as if the tight binding of K^+ ions is required to stabilize the altered selectivity filter.

Discussion

The potassium channel signature sequence TTVGYGD was first identified by Heginbotham et al. (Heginbotham et al., 1994) as critical for potassium selectivity. The residues fold as an extended loop (the P-loop) and is part of the P-region, about 20 residues of conserved sequence located between the S5 and S6 helices. We use here a system of numbering the entire linking region between S5 and S6, as identified in Shaker by Miller (Miller, 1990). The P-loop (residues 24'-30' in this numbering, TTVGYGD) forms four ion binding sites (Doyle et al., 1998) through which K^+ ions and water molecules can pass sequentially in a knock-on fashion. The geometry and flexibility is finely tuned to allow high K^+ selectivity with a high transport rate (Noskov & Roux, 2006; Roux, 2005).

In this paper we have considered the ion occupancy and conformation of the P-region under four conditions: the conducting state, a C-type inactivated state, the channel blocked by dendrotoxin, and in the absence of permeant ions. In the conducting state, the cryo-EM structure of our rat Kv1.2 construct (Kv1.2s) in DDM detergent micelles agrees with the crystal structure of Long et al. (2005) and is very similar to the structure of *Drosophila* Shaker in lipid nanodiscs (Tan et al., 2022). Also, apart from local differences in the chimeric region of the voltage sensor domains (VSDs), we confirm the observation (Long et al., 2007) that the rat Kv1.2 structure is essentially identical to the structure of the rat Kv1.2-2.1 paddle chimera as obtained from X-ray crystallography. In turn, the structure from cryo-EM imaging of Kv1.2-2.1 channels in lipid nanodiscs (Matthies et al., 2018) is also nearly identical. Thus the conformation of the entire transmembrane region of the Kv1.2 channel and its variants appears to be remarkably insensitive to its environment, whether lipid or detergent.

Inactivation

After the opening of the intracellular activation gate formed by the S6 helices, C-type inactivation (Hoshi et al., 1991) causes channel currents to switch off spontaneously. The inactivation process is very sensitive to mutations in the selectivity filter and nearby residues of the P-region and is influenced by the state of the S6 gate (Cuello et al., 2017; Li, Shen, Rohaim, et al., 2021) and the VSDs (Bassetto et al., 2021; Conti et al., 2016). Low K^+ concentrations, especially in the extracellular solution, accelerate inactivation (Levy & Deutsch, 1996).

Is C-type inactivation a reflection of selectivity filter instability? Sauer et al. (2011) investigated the structural stability of a channel selectivity filter, using a model system based on the NaK prokaryotic nonselective channel (Shi et al., 2006). NaK's selectivity filter (P-loop sequence TVGDGN) has only two ion binding sites, and opens into a wide extracellular vestibule. A similarly wide vestibule is seen in the nonselective HCN1 channel (Lee & MacKinnon, 2017; Shi et al., 2006) (**Figure 6**). NaK can however be converted to a highly K^+ selective channel, termed NaK2K, through just the two mutations D28'Y and N30'D, yielding the P-loop sequence TVGYGD. NaK2K has the four-site selectivity filter seen in all K^+-selective channels, and the residues Y28' and D30' participate in a hydrogen-bonded network to stabilize the selectivity filter just as in KcsA channels (Doyle et al., 1998). Y28' also participates in hydrophobic packing interaction. The

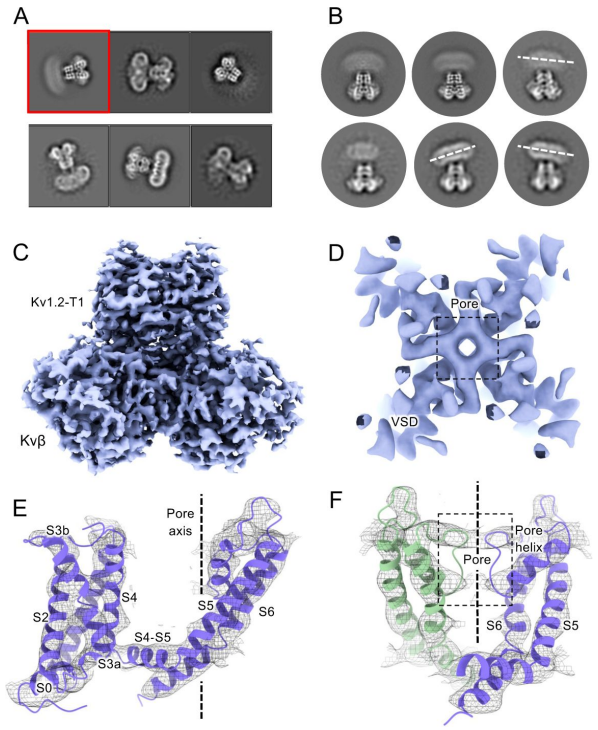

Figure 5.

Cryo-EM analysis of Kv1.2 W366F in Na+. (A) Representative 2D classes. (B) Second round of classification of first class in (A), outlined in red. Wobbling of the transmembrane domain is illustrated by the white dashed lines. (C) Density of intracellular domain, obtained by focused refinement. (D) Top view of TMD reconstruction, with resolution 7.0Å. (E) Overall TMD map density fits with the Kv1.2 W366F model, shown as ribbons. (F) There is low density in the selectivity filter (dashed rectangle).

removal of any of these interactions results in a loss of selectivity, and unraveling of the selectivity filter, returning to the large vestibule seen in NaK channels. Sauer et al. (2011) conclude that the standard four-ion-site, K^+ selective configuration of potassium channel selectivity filters is an energetically unfavorable, strained backbone conformation, and the weakening of the specific interactions that hold it in place lead to its unraveling, producing a lower-energy configuration that yields a nonselective conduction path. Similarly, the removal of K^+ ions from NaK2K destabilizes the selectivity filter, resulting in large fluctuations of the outer pore (Matamoros et al., 2023).

The H-bond interactions involving Y28' and D30' are also key to C-type inactivation in Shaker channels. Weakening those interactions produce channels that inactivate quickly or are found permanently inactivated (Pless et al., 2013). It is therefore no surprise that the loosening of H-bond restraints, resulting in the unraveling of the selectivity filter, yields a preferred, low-energy conformation with a large extracellular vestibule for the inactivated state of Kv channels.

In the case of Kv1.2, structural and molecular-dynamics studies have focused on the mutation W17'F (W366F in Kv1.2) which induces an inactivation-like process that is slowed in the presence of extracellular K^+ ions or pore blockers. In Shaker this mutation (W434F) causes the near total loss of open-channel current (Li et al., 2018; Perozo et al., 1993; Yang et al., 1997); in Kv1.2 it greatly accelerates inactivation (Suarez- Delgado et al., 2020). A large expansion of the outer selectivity filter in W17'F mutants is seen in structures of Shaker (Tan et al., 2022), Kv1.2-2.1 channels (Reddi et al., 2022) and also in Kv1.2 as reported here. Quantified as the distance between the diagonally-positioned Y28' alpha-carbons, the expansion in Shaker is from 8.6 to 12.8 Å. In both the Kv1.2-2.1 paddle chimera (Reddi et al., 2022) and in Kv1.2s the expansion is approximately from 7.2 to 10.7 Å. The expanded outer pore is very similar to the large extracellular vestibules observed in NaK and HCN1 channels (Fig. 7).

A striking feature of the inactivated state structure reported by Tan et al. (Reddi et al., 2022; Tan et al., 2022) is the high occupancy by potassium ions of the two remaining binding sites IS3 and IS4. During normal conduction, ion binding sites in the selectivity filter are usually occupied by K^+ and water molecules in alternation (Morais-Cabral et al., 2001). However, in molecular-dynamics simulations based on their Shaker W434F structure, Tan et al. (Tan et al., 2022) observed with high probability the simultaneous occupancy of IS3 and IS4 by two K^+ ions. The ions did not leave the sites during a (relatively long) 2 μs simulation with 300mV membrane potential applied, but knock-on permeation events were observed at a low rate, two events during 1μs, at the very high potential of 450 mV. A similar result was observed in earlier MD simulations of the Kv1.2-2.1 chimera where the W17'F mutation was artificially introduced (Conti et al., 2016; Kondo et al., 2018). Those simulations did not show the large rearrangement of the outer pore, but they did demonstrate small shifts in the geometry of IS3 and IS4 that, like those seen by Tan et al., produced simultaneous occupancy by K^+ ions and blockage of ion permeation. We also see strong ion densities in the two remaining ion binding sites in the Kv1.2s-W17'F channel (**Fig. 2E**, **Fig. 4E**), and a similar tight binding of adjacent K^+ ions seems also to block K^+ permeation in the structure of an inactivated Kv1.3 channel (Liu et al., 2021).

In a study of the Shaker mutant W17'F, Yang et al. (1997) observed, with symmetrical high K+ concentrations to maximize channel activity, brief (1 ms) openings of channels that occurred with a peak open probability of 10^{-5} immediately following a large depolarization to +80 mV (Yang et al., 1997). When open, the single-channel currents were the same magnitude as the currents in wildtype channels. It is unlikely that these currents arose from very slow ion conduction through destabilization of the tightly-bound K^+ ions in the inactivated configuration. Instead, the simplest explanation is that these currents arise when structural fluctuations transiently reconstitute the normal four-site selectivity filter, and the channel conducts normally for brief intervals. The normal selectivity filter is expected to be stabilized by bound K^+ ions. In the absence of external potassium ions the peak open probability drops to about 10^{-7} (Yang et al., 1997).

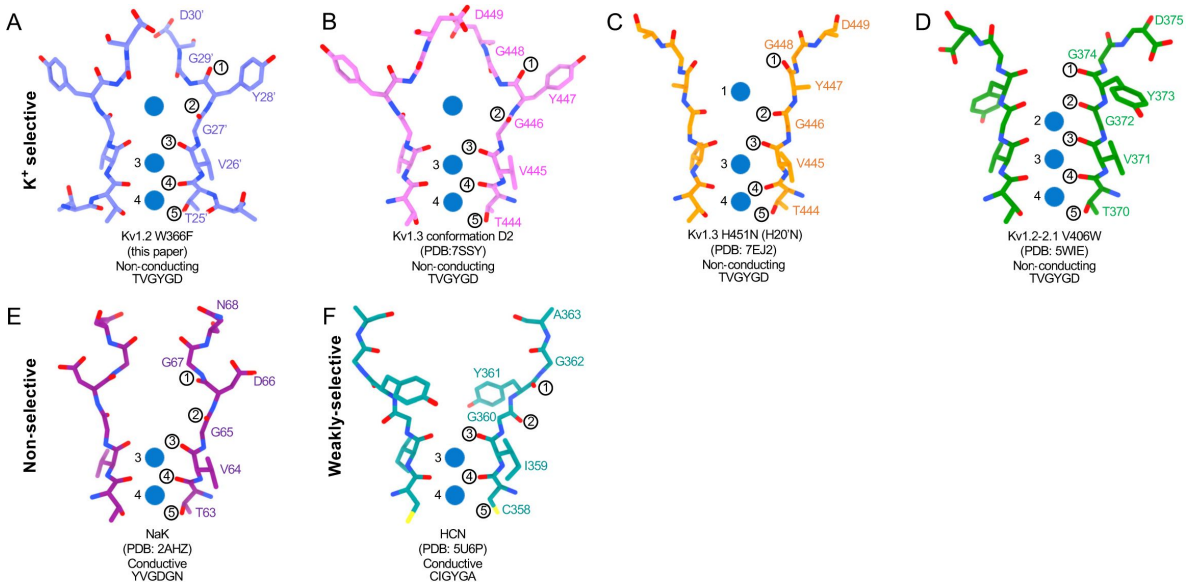

Figure 6.

Structural comparison of Kv1.2 W366F with various channel pores.

A-D, Selectivity filter structures and P-loop sequences of potassium selective non-conducting channels: (A) Kv1.2$_S$ W366F, (B) Kv1.3 alternate conformation, (C) Kv1.3 H451N, (D) Kv1.2-2.1 V406W. E-F, Pore regions of less-selective channels: the non-selective, conducting NaK (E) and the weakly-selective, conducting HCN (F). Potassium ions are shown as blue balls. Circled numbers enumerate the pore-forming carbonyl oxygens; carbonyl 2 faces the adjacent subunit in the clockwise direction in all but the HCN channel in panel F.

Are the structures of the various W17'F channels valid models for C-type inactivation? In recent cryo-EM studies (Selvakumar et al., 2022) the human Kv1.3 channel was found to spontaneously exist in one or two alternative conformations that appear to be inactivated states. The D1 conformation shows a large displacement of D30' and is reminiscent of the cryo-EM structure of the Kv1.3 rapidly-inactivating mutant H20'N (Liu et al., 2021). It exhibits a partially twisted P-loop (**Figure 6** and **Figure 6—figure supplement 2B**) as if it were an intermediate state between open and the W17'F structures. Meanwhile the D2 conformation is very similar to that of the W17'F variants considered here. This strongly supports the widely-held view that these mutant channels are in a conformation close to, if not identical to, a true C-type inactivated state.

Why is inactivation much more complete in the Shaker mutant W17'F than in Kv1.2 or Kv1.2-2.1? Clearly one can compare the stabilities of the conducting and the inactivated conformations. Wu et al. (2022) mutated several of the residues that form important interactions in these channels, and found that the inactivation behaviors of Kv1.2 and Kv1.2-2.1 are different from that of Shaker. In the conducting state, the H-bond networks stabilizing the key residues Y28' and D30' in Shaker and Kv1.2 very similar, with the only obvious difference being at position 22' where Shaker has Thr but Kv1.2 has Ser. It turns out that the mutation S22'T in the Kv1.2 background has little effect on inactivation; thus to a first approximation the conducting state is equivalently stabilized.

In the inactivated state structures, all obtained with the W17'F mutation, a variety of H- bond interactions arise in the linker sequence between the P-loop and the S6 helix, with the variety arising from different conformations of Loop 1 and Loop 2, two regions of the linker (**Figure 6—Figure Supplement 1**). Details of the interactions are discussed in the Figure legend. We conclude that a quantitative evaluation of the stability of the inactivated state will require more than simply an enumeration of H-bonds in this region of the protein sequence.

Block of the channel by dendrotoxin

Potassium currents can be inhibited by five distinct families of toxins. The spider toxins Hanatoxin, SGTx1 and VSTx1 interact with the voltage sensors of Kv channels to inhibit voltage-dependent channel activation (Lee & MacKinnon, 2004; Wang et al., 2004).

Other toxins bind directly to the extracellular mouth of the channel to block current. The cone-snail toxin Cs1 binds to the extracellular surface of Kv channels and is thought to block currents by inducing a conformational change in the protein, collapsing the selectivity filter (Karbat et al., 2019). In X-ray crystal structures the scorpion toxin Charybdotoxin is seen to block Kv1.2-paddle chimera channels by inserting a lysine residue directly into the selectivity filter, disrupting the ion-binding site IS1 to inhibit ion flow (Banerjee et al., 2013). The same mechanism holds for block of Kv1.3 by the sea anemone toxin ShK as studied by cryo-EM (Selvakumar et al., 2022); in all three cases the lysine terminal amine interacts with the Y17' carbonyls which form the top of binding site IS1. We now report that Kv1.2 block by the snake toxin α-Dendrotoxin (α-DTx) is by a similar mechanism.

Obtaining the structure of an asymmetric ligand bound to a four-fold symmetric channel, is challenging, and the four structural studies that have been done have used different strategies. In their X-ray crystallographic study, Banerjee et al. (2013) were able to interpret and model at low resolution the four-fold superimposed toxin density, using heavy-atom derivatives in a series of crystal structures to establish the pose of the toxin molecule. The difficulty of modeling the CTx molecule precluded assigning a precise location to the Lys22 channel-blocking sidechain; nevertheless, in the 2.5 Å map of the selectivity filter are seen three well-resolved, discrete ion densities in the sites IS2, IS3 and IS4, and the authors conclude that the toxin interaction prevents ion occupancy of the IS1 site. A cryo-EM study that yielded a similar C4 symmetric reconstruction of Kv1.3 with bound dalazatide, a derivative of the ShK toxin, was obtained by Tyagi et al. (2022). The C4-symmetric reconstruction did not yield an interpretable map of the toxin, but clear ion densities in IS2, IS3 and IS4 were visible.

Selvakumar et al. (2022) also obtained a structure of ShK bound to Kv1.3, but in this case the ShK toxin was fused to a Fab fragment; this yielded an asymmetric ligand large enough to allow C1 reconstruction from the cryo-EM images. The resulting 3.4Å map allowed the toxin K22 sidechain to be modeled entering the pore and extending to near the Y17' carbonyl oxygens.

From our cryo-EM data we obtained a C1 map of α-DTx bound to Kv1.2s at 3.2 Å; this was done by extensive image processing and was helped by the larger size of α-DTx (59 residues as compared to 35 for ShK). With this map the side chain of the toxin residue K5 could be traced, apparently with the terminal amine directly coordinated by the Y17' carbonyls. A surprise in this map are the positions of the K^+ ion peaks in the selectivity filter (**Figure 4E**). Ion density is visible in IS3, and somewhat lower density is seen in IS1; there is no density peak in IS2. The different pattern of ion densities with DTx compared to CTx, having two rather than three peaks in the selectivity filter, implies that the interaction between the lysine side chain and the selectivity filter is in some way different in DTx compared to the other toxins.

The selectivity filter in the absence of K^+

In the absence of K^+, large voltage-dependent Na^+ currents are observed in wildtype Kv2.1 channels (Korn & Ikeda, 1995) and in Shaker channels (Melishchuk et al., 1998). The Kv1.2 structure reported here with Na^+ replacing all K^+ in the solution shows a selectivity filter conformation that is little changed from the K^+ structure (**Figure 5B**). Na^+ ion densities are seen in the ion-binding sites, but the limited resolution precludes an analysis of the coordination of the Na^+ ions.

The Shaker-W17'F channel in the absence of K^+ stably carries large Na^+ and Li^+ currents (Starkus et al., 1997). These currents are blocked by low concentrations of K^+, and this would be expected as potassium binding to the sites IS3 and IS4 in this mutant is very tight (Tan et al., 2022). We therefore sought to obtain the structure of the corresponding Kv1.2-W17'F channel in Na^+ solution (**Figure 5**). In 2D classes the complex appeared to be highly unstable, with large variations in the "wobble" angle between the transmembrane and cytoplasmic domains. Attempts to recover the structure of the transmembrane region by focused refinement yielded only low- resolution structural information. We conclude that this channel, at least as solubilized in detergent, has a highly unstable conformation when K^+ ions are absent.

Methods

Kv1.2-Kvβ expression and purification

The rat Kv1.2 alpha-subunit constructs were derived from that of Long et al. (2005), having the full-length (GenBank: X16003) sequence containing the mutation N207Q to eliminate a glycosylation site. Our Kv1.2s construct contained the additional mutations L15H and G198S in unstructured regions; the inactivating construct contained the further mutation W366F. To each of these was added at the N-terminus two tandem Strep tags (sequence WSHPQFEK) separated by a Gly-Ser linker. The beta-subunit construct was derived from the rat beta2 core, residues 36-357 (Gulbis et al., 1999). To eliminate very strong electrostatic interactions between the many Lys residues on the "bottom" of the beta-subunits and the negatively-charged carbon film or graphene substrates, we mutated to glutamine the five lysine residues at positions 94, 104-106 and 258 of the beta2 subunit. The fold of the beta subunits containing these mutations is indistinguishable from the wildtype structure of Long et al. (2007).

To express both subunits in a single construct, Kv1.2 and Kvβ genes were separately inserted into pPicZ-B (Thermo-Fisher) vectors between the XhoI and AgeI sites in the multi-restriction-sites region. Subsequently the pPicZ-B vector carrying Kvβ was opened at BglII and BamHI restriction

sites, and the insert including the AOX1 promoter was inserted into the other pPicZ-B vector, upstream of the AOX1-driven Kv1.2 cDNA, at the BglII site.

The *P. pastoris* strain SMD1168 (Invitrogen) was electroporated with the pPicZ-B plasmids. YPDS (yeast extract, peptone, dextrose, and sorbitol) plates containing Zeocin (800 ug/ml) were used to select transformants. Stocks were stored in 15% glycerol at -80°C.

The expression and purification procedures were based on those of Long et al. (Long et al., 2005). Briefly, we inoculated 1 liter of BMGY medium (this and the other yeast media were obtained from Invitrogen) with 10 ml of an overnight culture grown in YPD medium with Zeocin (100 ug/ml). After centrifugation (5500× %, 10 minutes), the cells were transferred to BMMY medium including 0.5% (v/v) methanol and grown for 24 h. After adding an additional 0.5% methanol to increase protein expression, cells were grown for 2-3 days. Cells were centrifuged (5500× %, 20 minutes), the pellet was frozen and stored at -80°C.

Thawed cells were lysed at 4° in a French Press. One gram of cell lysate was resuspended in 5mL of Lysis buffer consists of 100 mM Tris-HCl (pH 8.0), 150 mM KCl, 300 mM sucrose, 5 mM EDTA, 0.05 mg deoxyribonuclease I, 1 mM MgCl2, 1 mM phenylmethylsulfonyl fluoride, 1 mg/ml each of leupeptin, pepstatin and aprotin, and 0.1 mg/mL of soy trypsin inhibitor. Lysis buffer plus 30 mM dodecylmaltoside (DDM) was used to solubilize the membranes for 3 hours at room temperature. Centrifugation (13000×*g*, 20 minutes) separated the unsolubilized material. The supernatant was added to Strep-Tactin Sepharose beads (IBA Lifesciences) preequilibrated with Membrane Resuspension Buffer (100 mM Tris-HCl pH 8.0, 150 mM KCl, 3mM TCEP, 5 mM EDTA, 10 mM beta-mercaptoethanol, and 5 mM DDM. The bead slurry (approximately 1 ml) was incubated 1h at 4°C with gentle rotation. A column was used to collect the beads after incubation, followed by washing with 14 volumes of Membrane Resuspension Buffer with added lipids (0.1 mg/ml of the mixture 3:1:1 of POPC:POPE:POPG). The addition of 10 mM desthiobiotin was used to elute the bound protein. The eluted protein was concentrated with a Millipore Amicon Ultra 100 K filter and further purified by size-exclusion chromatography (SEC) on a Superose S6 column pre-equilibrated with 20 mM tris-HCl (pH 7.5), 150 mM KCl, 2 mM TCEP, 10 mM DTT, 1 mM EDTA, 1 mM PMSF, 1 mM dodecylmaltoside (Anatrace, anagrade) and 0.1 mg/ml lipid mixture (3:1:1 of POPC:POPE:POPG). We pooled fractions containing both alpha and beta subunits, and when necessary concentrated the protein to 1~2 mg/ml (Amicon Ultra 100 KDa, Millipore). For experiments under K^+-free conditions, in the SEC buffer NaCl replaced KCl.

Oocyte expression and voltage-clamp recordings

The Kv1.2s alpha subunit or its W366F mutant construct was cloned into a pcDNA3.1 vector. RNA was prepared from the XbaI-linearized plasmid using T7 RNA polymerase. Xenopus oocytes were defolliculated by collagenase treatment, injected with cRNA and stored in ND96 solution (96 mM NaCl, 2 mM KCl, 1.8 mM CaCl2, 1 mM MgCl2, 5 mM HEPES, pH 7.4 with NaOH) at 18°C. Recordings were done at room temperature, 5-6 days post-injection in ND96 solution or KD96, the same solution but made with 96 mM KCl, 2 mM NaCl and KOH. Two-electrode voltage clamp recordings employed an OC- 725C amplifier (Warner Instruments).

Cryo-EM specimen preparation, data acquisition and processing

Quantifoil holey carbon grids (R1.2/1.3, 300 mesh, Au) were glow-discharged at 15 mA for 1 min with carbon side facing upwards in the chamber. The chamber of the freezing apparatus (Vitrobot Mark IV, Thermo Fisher Scientific) was preequilibrated at 16 °C and 100% humidity. A 3 μL droplet of protein sample was applied to the carbon side of each grid and blotted for 3 or 5 s with zero blotting force after 15 s wait time before plunge- freezing in liquid ethane. For the DTX bound sample, about 400nM α-DTX (Alomone Labs) was mixed with Kv1.2s protein 30 min prior to cryo-EM grid preparation.

For the Kv1.2s-Na^+, W366F-Na^+, and DTX-bound samples, graphene-covered grids were used to allow lower protein concentrations (0.05 to 0.1 mg/ml) to be used. These were prepared from commercial graphene (Trivial Transfer Graphene, single layer; ACS Material LLC) using the recommended transfer protocol and floated onto quantifoil grids. To make the graphene layer hydrophilic, grids were then plasma-cleaned (Gatan 950 Advanced Plasma System) under Ar/O2 at 10 W for 10 s with the graphene coated surface facing upwards in the chamber. Vitrification was conducted as described above but with 30 s wait time.

Cryo-EM samples were imaged on a Titan Krios cryo-EM (Thermo Fisher Scientific) operated at 300 keV, equipped with a Bio Quantum energy filter (20 eV slit width) and K3 camera (Gatan). Micrographs were collected using super-resolution mode, physical pixel size 1.068 Å, with SerialEM software (Schorb et al., 2019) using image shift patterns and one shot per hole. A total of 6335, 8310, 4507, 2572, 4680 micrographs were collected for WT, W366F, DTX-bound, Na^+ bound WT, and Na^+ bound W366F, datasets respectively.

Processing for each dataset is summarized in the Figure Supplements to **Figs. 1**-**4**. Beam-induced motion was corrected by MotionCor2 (Zheng et al., 2017) and CTF values were estimated by Gctf (Zhang, 2016). Particles were picked either by reference- free Laplacian-of-Gaussian autopicking; an adversarial-template-based program Demo Picker written by F.J.S.; or RELION reference-based auto-picking. All further processing used RELION 3.1. Picked particles were extracted and subjected to rounds of 2D and 3D classification before refinement. Transmembrane-domain masks were used for focused refinement to optimize the resolution of the transmembrane region. Beam-tilt and per-particle CTF refinement followed by per-particle motion correction were applied to further improve the resolution.

Analysis of the DTx-Kv1.2s complex started with a C4 reconstruction of the complex from 323k particles. We then performed a rough docking into the Kv1.2s apo density of a toxin map created from the 1DTX model. The toxin pose was chosen not to be inconsistent with the symmetrized toxin density visible in the DTx-Kv1.2s C4 map. Four of these composite maps were created, with the toxin pose rotated 90° each time about the z-axis. These were filtered to 20Å resolution for use as 3D references. Meanwhile a C4 symmetry expansion of the 323k particles was performed, resulting in a 1.294M particle stack. A soft cylindrical mask of radius 24 Å and height 48 Å was created, centered on the z-axis at the interface between the toxin and the pore region. Using this mask and the four 3D references, we performed 3D classification without alignment in RELION, and chose one of the four resulting classes as a C1 reconstruction of the masked region. Using the corresponding set of 312k particles we performed C1 homogeneous reconstruction in CryoSPARC to yield the refined structure at 3.2 Å resolution.

Protein model building, refinement and structural analysis

An Alpha-Fold predicted rat Kv1.2 model (alphafold.ebi.ac.uk/entry/Q09081) was used to build the Kv1.2 native atomic model. The W366F, DTX-bound, and Na^+-bound models were subsequently built from this Kv1.2 model. Model fitting was performed with the CCPEM program suite. Initial docking was performed with Molrep; obvious outliers of were manually fixed in Coot 0.9 (Emsley et al., 2010) and real space refinement used Refmac 5 (Murshudov et al., 2011) and Phenix (Liebschner et al., 2019). Density map rendering, analysis and figure preparation were done with UCSF Chimera and ChimeraX (Goddard et al., 2018; Pettersen et al., 2004).

Acknowledgements

We thank Marc Llaguno and Jianfeng Lin for aid with microscopy for screening on the Glacios microscopes, and Shenping Wu for aid with the Titan Krios data collection. We are grateful to Yufeng Zhou (University of Pennsylvania) and David Fedida (University of British Columbia) for

providing the original constructs and consultation on expression constructs.

Funding

This research was funded by NIH grant NS021501. CryoEM imaging was performed in the Yale Cryo-EM facilities, which are supported in part by NIH grant S10OD023603

Author contributions

Yangyu Wu, Data curation, Formal analysis, Investigation, Methodology, Writing - original draft; Yangyang Yan and Youshan Yang, Data curation, Formal analysis, Investigation, Methodology; Shumin Bian, Alberto Rivetta and Ken Allen, Methodology; Fred Sigworth, Conceptualization, Formal analysis, Supervision, Validation, Funding acquisition, Project administration, Writing – review and editing.

Data availability

The cryo-EM maps and atomic models for this work have been deposited in the Electron Microscopy Data Bank (*https://www.ebi.ac.uk/pdbe/emdb/*) and in the Protein Data Bank (*https://www.rcsb.org*). The data are available under the following accession codes: Kv1.2 open (EMD-43134, PDB 6VC6), Kv1.2-W366F inactivated (EMD-43136, PDB 6VCH), Kv1.2-DTx toxin-blocked (EMD-43131, PDB 6VC3) and Kv1.2 in Na^+ (EMD-43133, PDB 6VC4). The particularly challenging cryo-EM dataset of Kv1.2- W366F in Na^+ will be deposited in the Electron Microscopy Public Image Archive.

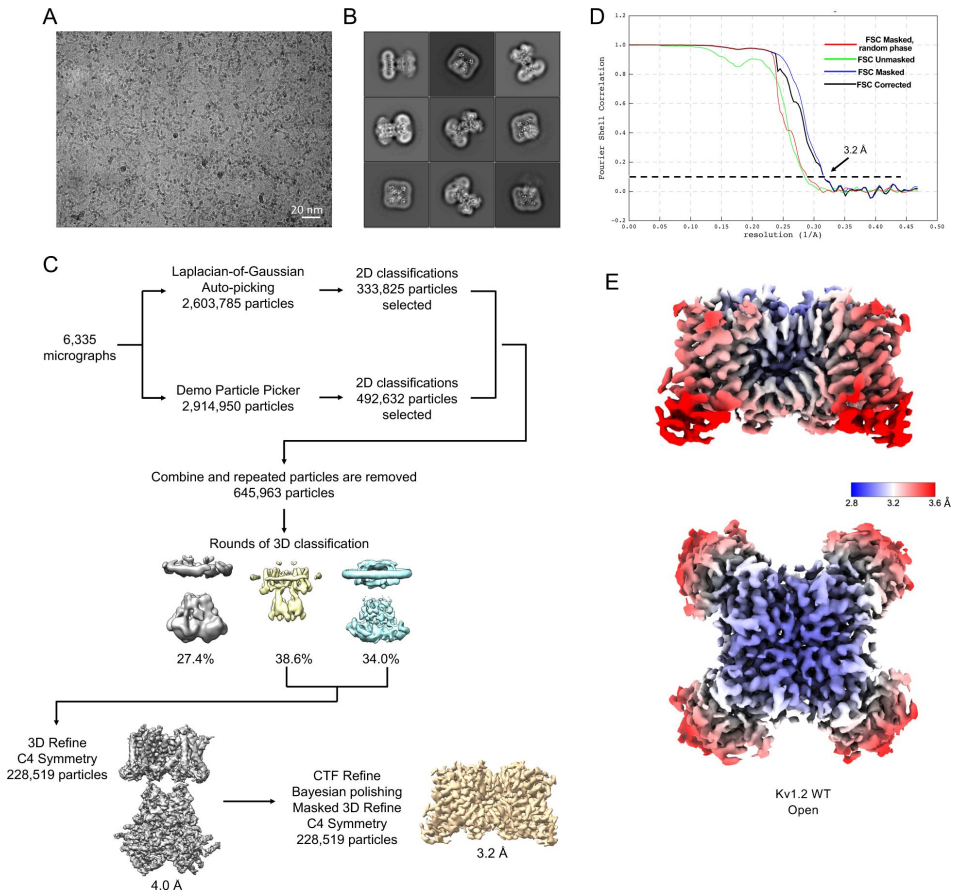

Figure 1 - figure supplement 1.

Image processing and reconstruction of Kv1.2s.

(A) Representative micrograph. (B) Representative 2D classes. (C) Cryo-EM data processing workflow. (D) Gold standard FSC resolution estimation. (F) Local resolution estimation.

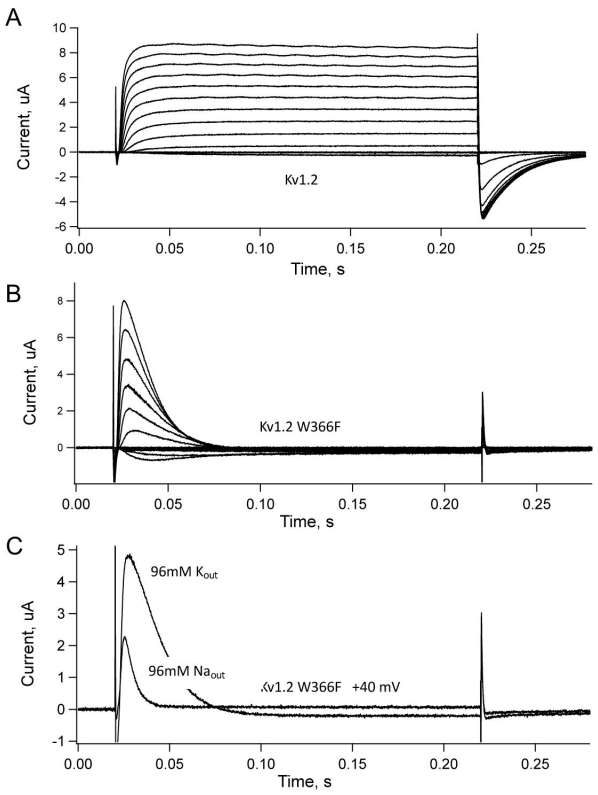

Figure 2 - figure supplement 1

currents from native and W366F Kv1.2 channels.

Xenopus oocytes were injected with mRNA for the alpha subunit constructs used in this study. **A**, native Kv1.2 currents elicited from pulses to -60 to + 60mV in 10 mV steps, from a holding potential of -80mV. **B**, Same voltage protocol applied to channels with W366F alpha subunits, recorded with 96 mM K^+ bath solution. **C**, Comparison of currents elicited from an oocyte at +40 mV with 96mM K^+ or Na^+ bath solutions. The potassium-free Na^+ solution yielded faster inactivation, as expected for C-type inactivation. The apparently sustained current in 95 mM Na^+ solution is an artifact of P/4 leak subtraction at -120mV holding potential.

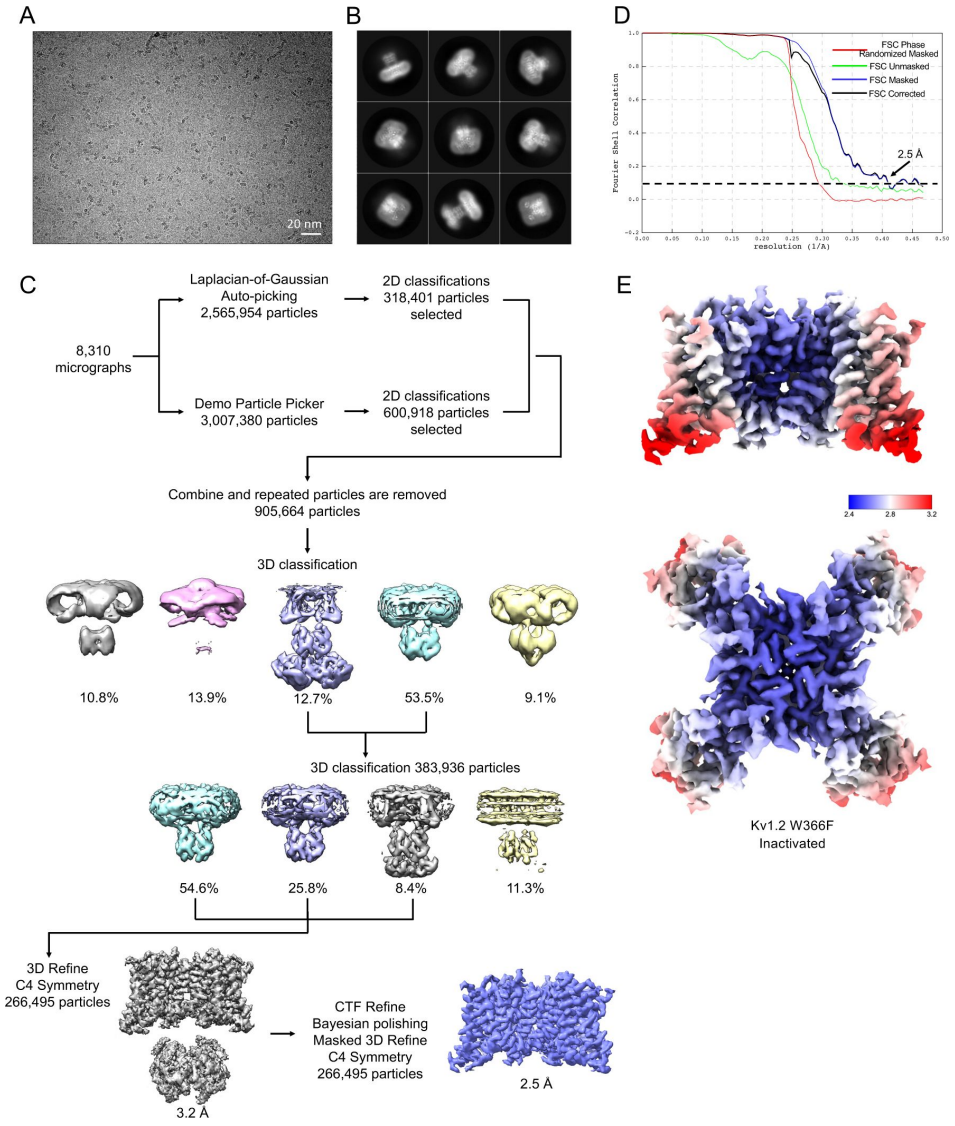

Figure 2 - figure supplement 2

, Processing of Kv1.2 W366F images. (A) Representative micrograph. (B) Representative 2D classes. (C) Cryo-EM data processing workflow. (D) Gold standard FSC resolution estimation. (F) Local resolution estimation.

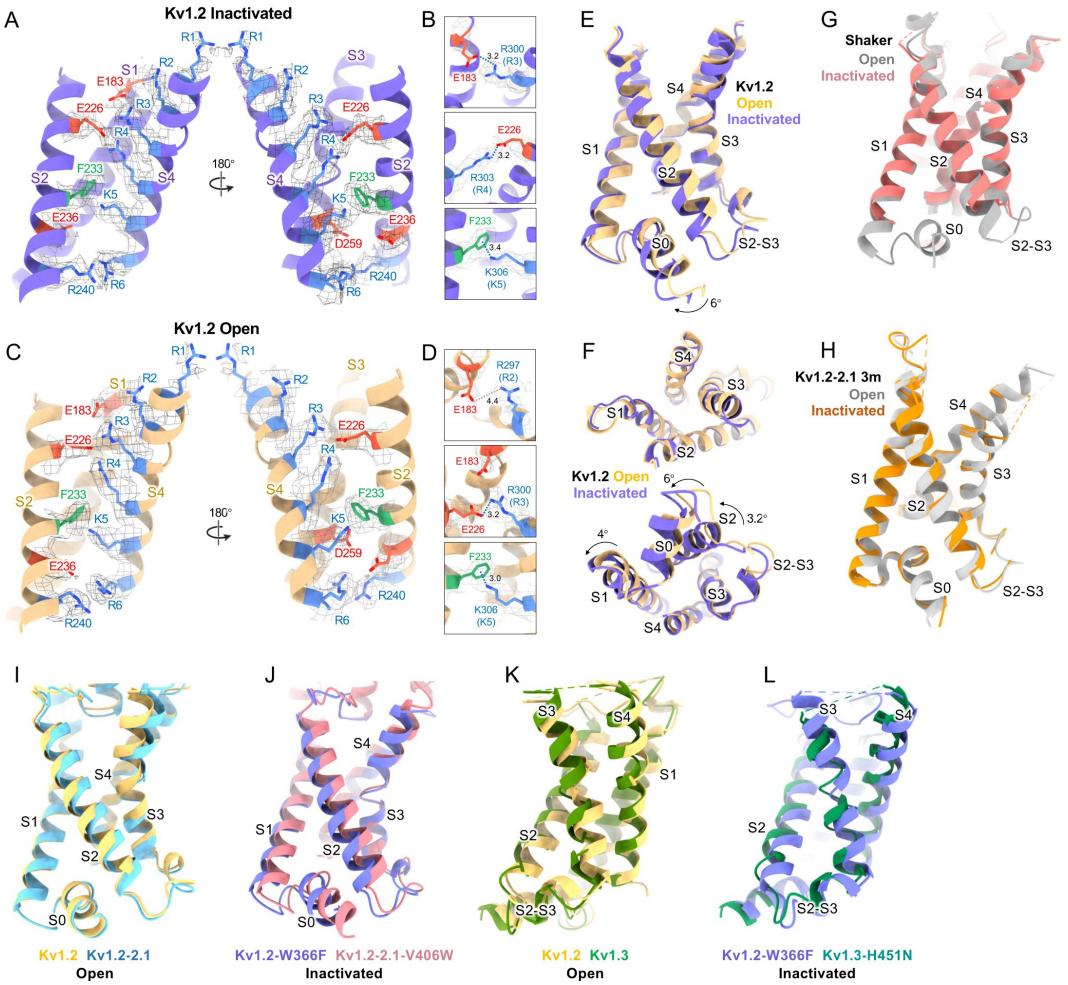

Figure 2 - figure supplement 3.

Voltage-sensing-domain conformational differences between open and C-type inactivated states. Side view of VSD structures and maps of Kv1.2s in (A) inactivated state. (B) Kv1.2s VSD R3/E183 (upper), R4/E226 (middle), and K5/F233 (lower) interactions in the inactivated state. VSD structure in open state. (D) VSD relative position of R2/E138 (upper) and R3/E226 (middle), K5/F233 (lower) interactions in the open state. Positively charged and negatively charged residues are shown in blue and red, while aromatic residues are shown in green. Side view (E), top view (F, upper) and bottom view (F, lower) VSD conformational difference between open (yellow) and inactivated (purple) states. Superposition of (G) Shaker open (PDB: 7SIP), Shaker W434F inactivated (PDB: 7SJ1) and (F) Kv1.2-2.1 open (PDB: 7SIZ), Kv1.2-2.1 3m inactivated (PDB: 7SIT) VSD structures. (I-L) Superposition of VSD structures. (I) Kv1.2$_S$ (yellow) and Kv1.2-2.1 (light blue, PDB: 2R9R); (J) Kv1.2s W366F (purple) and Kv1.2-2.1 V406W (carnation, PDB: 5WIE); (K) Kv1.2 (yellow) and Kv1.3 (green, PDB: 7EJ1); (L) Kv1.2 W366F (purple) and Kv1.3 H451N (clover, PDB: 7EJ2).

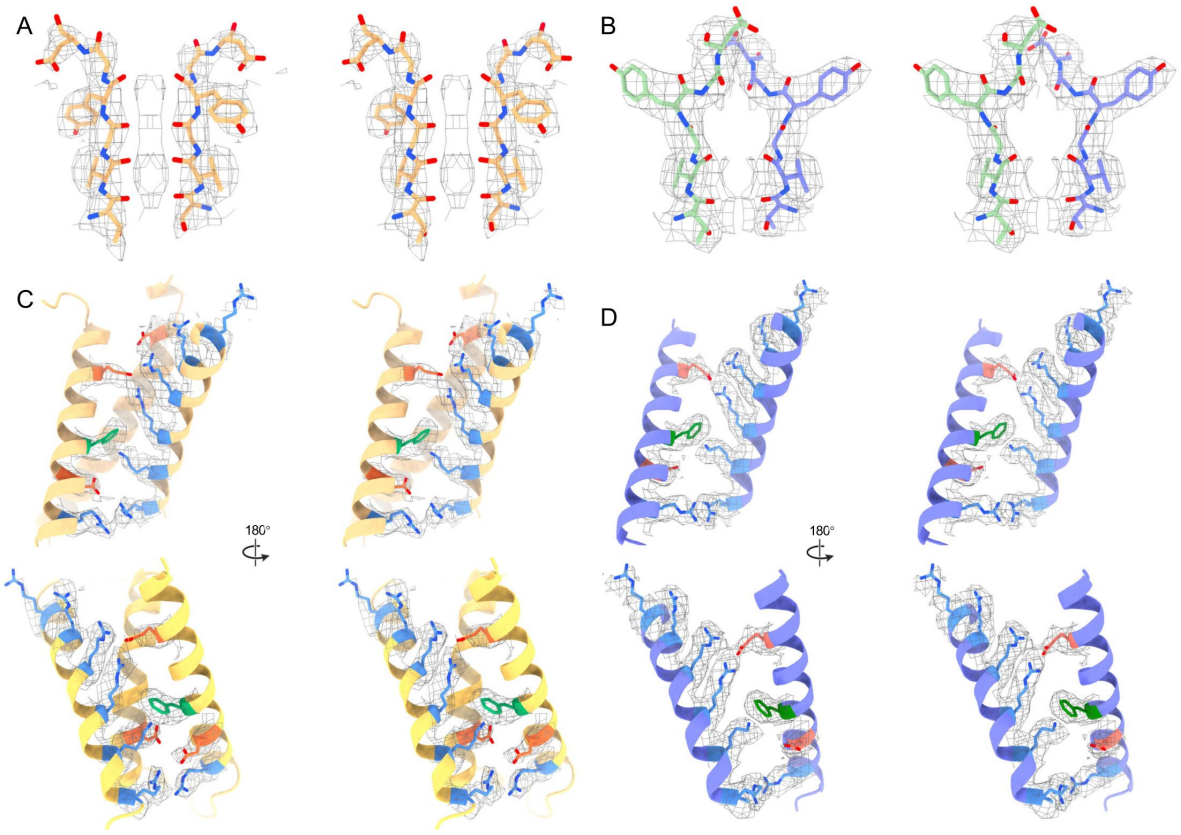

Figure 2 - figure supplement 4

Stereo views of selectivity filter and voltage-sensing-domain. Stereo view of (A) Kv1.2s SF, (B) Kv1.2s-W366F SF, (C) Kv1.2s VSD, (D) Kv1.2s-W366F VSD.

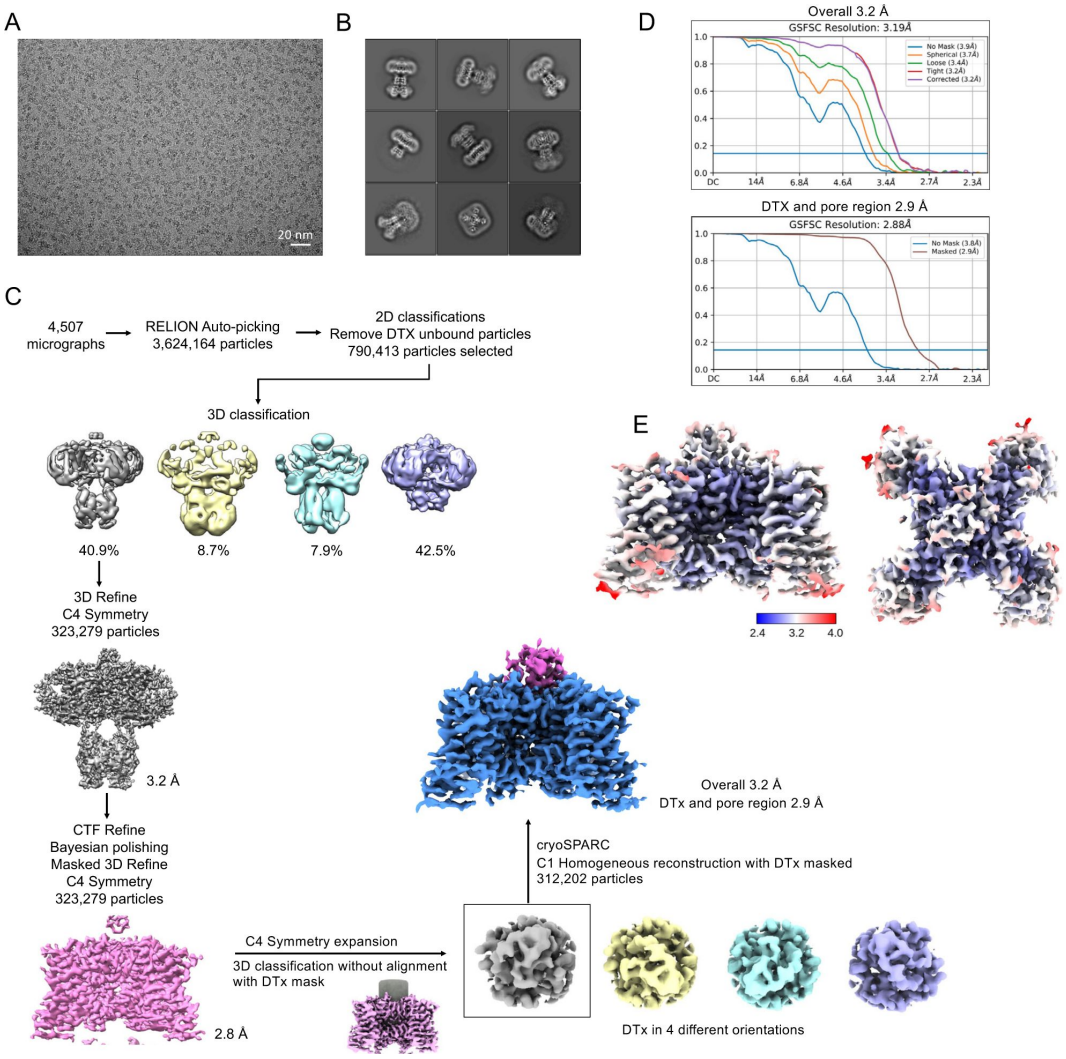

Figure 3 - figure supplement 1.

Cryo-EM imaging and reconstruction of Kv1.2s-DTX.

(A) Representative micrograph. (B) Representative 2D classes, showing the DTx “cap” on the particles. (C) Cryo-EM data processing workflow. See Methods for details of the symmetry expansion and C1 reconstruction. (D) Gold standard FSC resolution estimation for the overall map (top) and the DTX-plus-selectivity filter masked region. (E) Local resolution estimation.

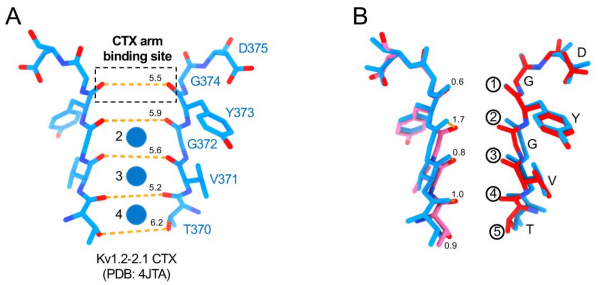

Figure 3 - figure supplement 2

Comparison of the Kv1.2-2.1 CTx bound selectivity filter with the Kv1.2s DTx-bound structure. (A) Side view of the selectivity filter of Kv1.2-2.1 CTx bound conformation (Banerjee et al. 2013). Orange dashed lines show the distances between carbonyl oxygens, for comparison with **Fig. 3G**. Potassium ions are shown as blue balls. (B) Superposition of Kv1.2 DTx (red) and Kv1.2-2.1 CTx (blue) selectivity filter structures. Apparent carbonyl displacements are given in Å.

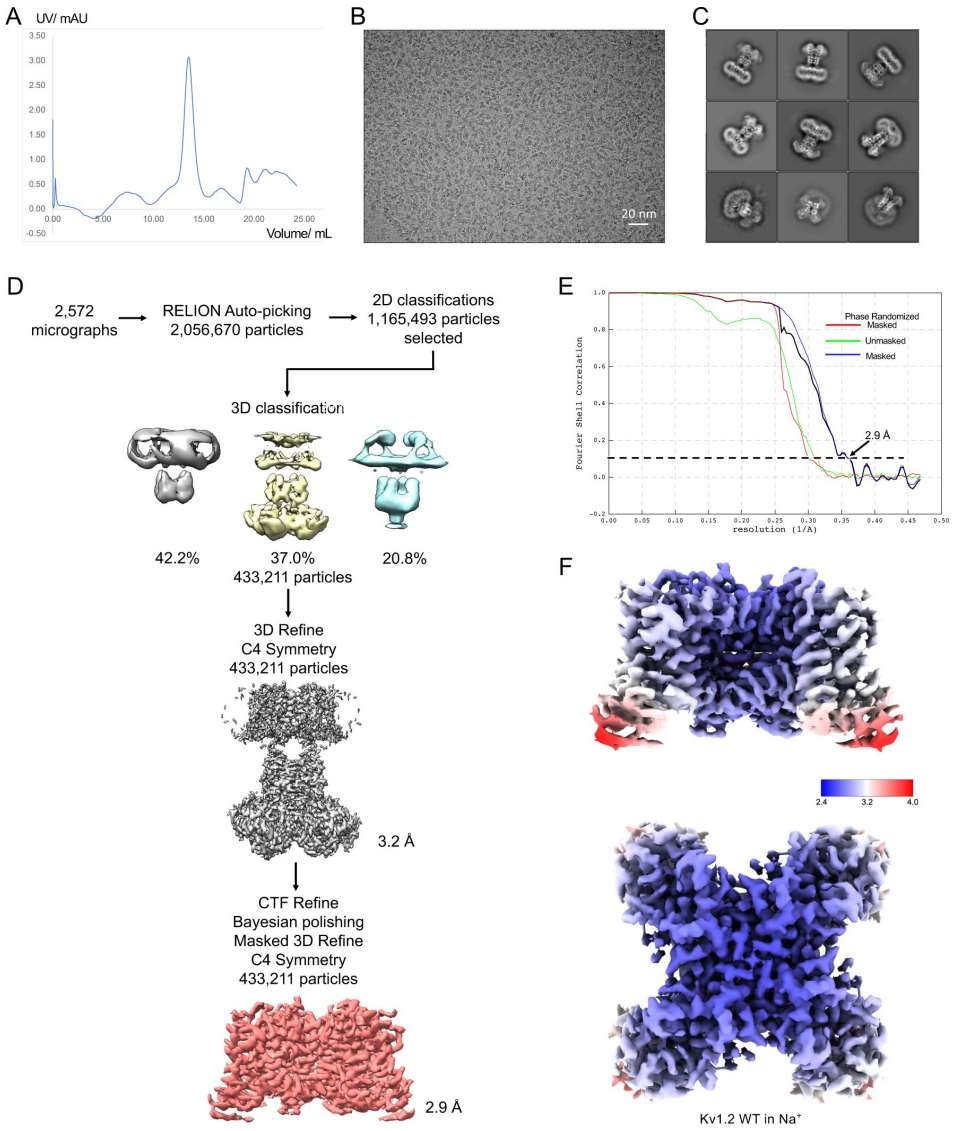

Figure 4 - figure supplement 1

Cryo-EM of Kv1.2s in Na+. (A) Size-exclusion chromatogram. Detector drift was large compared to a small protein signal. (B) Representative micrograph showing monodisperse particles on the graphene substrate. (C) Representative 2D classes. (D) Cryo-EM data processing workflow. (E) Gold standard FSC resolution estimation. (F) Local resolution estimation.

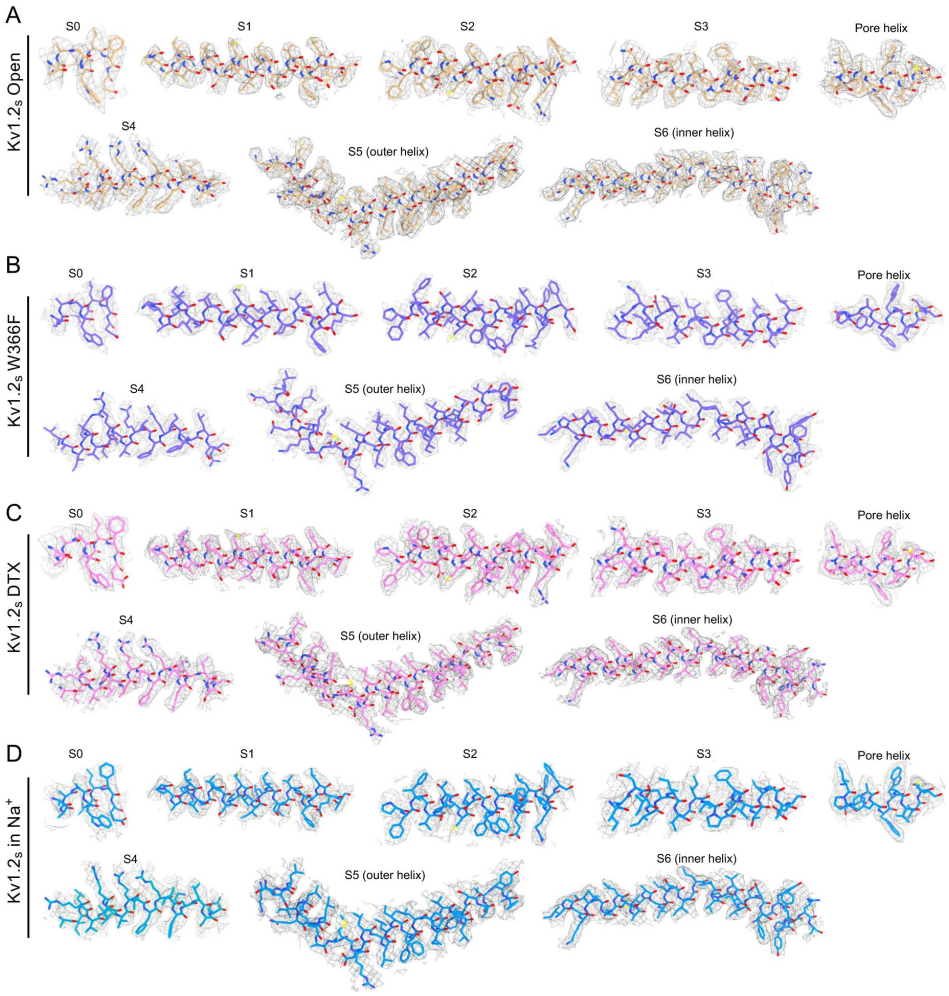

Figure 4 - figure supplement 2.

Comparisons of cryo-EM density map and model for alpha helices in each Kv1.2 structure reported here.

	Kv1.2-open	Kv1.2-W366F	Kv1.2-DTx	Kv1.2-Na+	Kv1.2-W366F-Na+
Data collection and processing					
Microscope			FEI Titan Krios		
Detector			K3		
Voltage (kV)			300		
Electron exposure (e-/Å^2)			50		
Magnification			81000		
Defocus range (um)			-1.0 to -2.0		
Pixel Size (Å/pixel)			1.068		
Symmetry imposed	C4	C4	C1	C4	C4
Micrographs (no.)	6335	8310	4507	2573	9628
Map resolution (Å)	3.2	2.5	3.2	2.8	7.8
Final particle images (no.)	228519	266495	312202	433211	239100
FSC threshold			0.143		
Refinement					
PDB codes	6VC6	6VCH	6VC3	6VC4	
EMDB codes	43134	43136	43131	43133	
Map sharpening B factor (Å^2)	-185.2	-50	-116.8	-157.8	
Model Composition					
Chains	4	5	6	4	
Atoms	7740	7614	8219	7740	
Residues	1028	1012	1087	1028	
Water	0	0	0	0	
Ligands	0	K: 2	K: 2	0	
Bonds (RMSD)					
Length (Å)	0.003 (0)	0.004 (0)	0.002 (0)	0.003 (0)	
Angles (°)	0.562 (0)	0.577 (0)	0.484 (0)	0.621 (0)	
Validation					
Molprobity score	1.52	1.37	1.43	1.55	
Clashscore	7.58	5.83	7.03	8.1	
Poor rotamers (%)	0.26	0.65	0.24	0.56	
Ramachandran plot					
Favoured (%)	97.51	97.77	97.83	97.91	
Allowed (%)	2.49	2.23	2.17	2.09	
Outliers (%)	0.00	0.00	0.00	0.00	

Figure 4 - figure supplement 3

Cryo-EM data collection, refinement and validation statistics

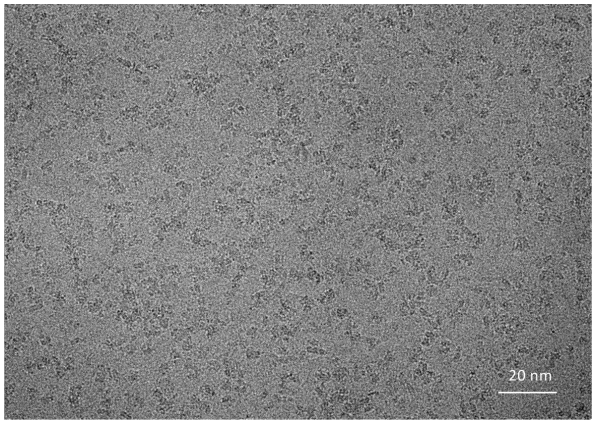

Figure 5 - figure supplement 1

Representative micrograph of Kv1.2 W366F in Na+, demonstrating the absence of protein aggregates on the graphene substrate.

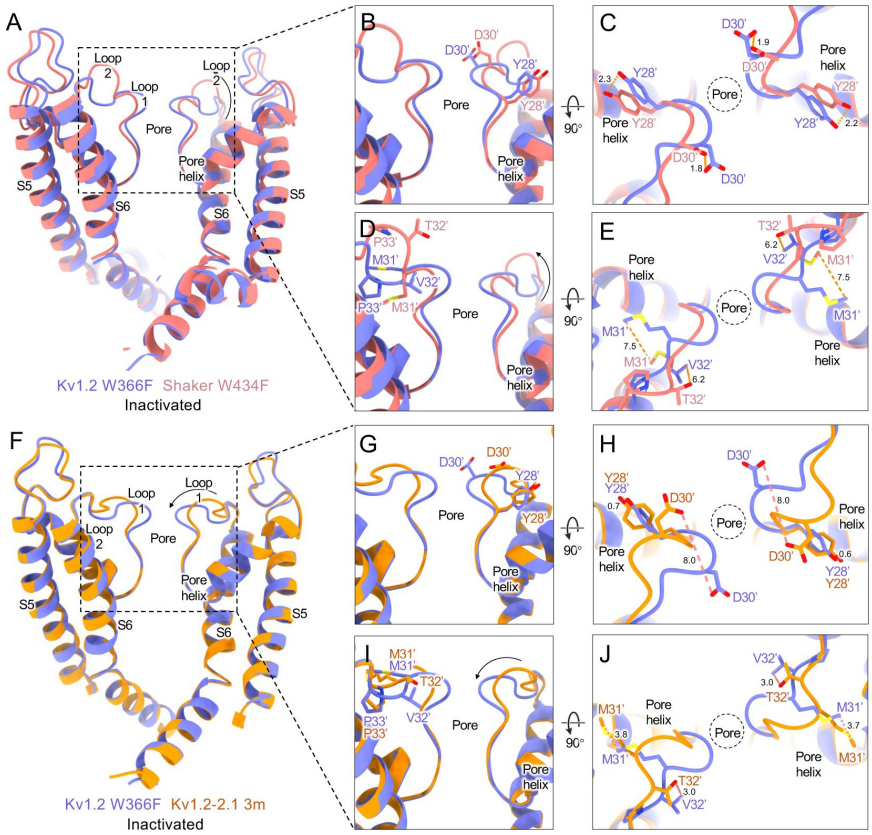

K	Asp	Val/Thr	Loop1	Loop2	H-bonding
Kv1.2 W366F	D28'-flipped	V32'	unflipped	flipped	Inter/intra-subunit
Shaker W434F	D28'-flipped	T32'	unflipped	flipped	Intra-subunit
Kv1.2-2.1 3m	D28'-not flipped	T32'	flipped	unflipped	Inter-subunit

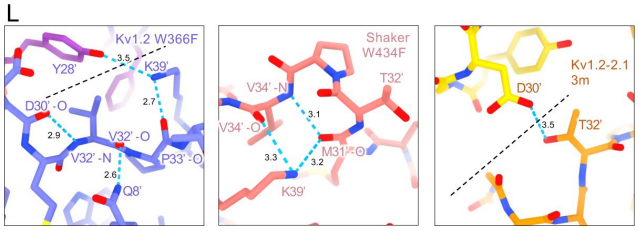

Figure 6–Figure Supplement 1.

Structural comparison of inactivated Kv channels.

(A-J) Structural superposition of Kv1.2s-W366F pore domain with other inactivated channels: side view with Shaker W434F (A) or Kv1.2-2.1-3m (F). Loop 1 conformational differences with Shaker W434F side view (B), top view (C); or with Kv1.2-2.1-3m side view (G), top view (H). Loop 2 conformational changes with Shaker W434F side view (D), top view (E); Kv1.2-2.1 3m side view (I), top view (J). (K) Table lists of the differences among the inactivated Kv channels. (L) H-bonds among the inactivated Kv channels. Adjacent subunits are shown as different colors, and a dashed black line denotes the subunit boundary. H-bonding patterns affect the stability of the inactivated state and an obvious difference is at the location 32', where Shaker has Thr and Kv1.2 has Val. The mutation V32'T in the Kv1.2-2.1 background provides a new hydrogen bond that stabilizes the important residue D30' in the inactivated conformation; this can be seen in the Kv1.2-2.1-3m structure (L, panel 3). Our inactivated Kv1.2s structure (containing V32') nevertheless shows an H-bond network that includes Y28' and D30' along with main-chain atoms, possibly yielding a similar stabilization of the inactivated state (L, panel 1). The inactivated Shaker structure lacks H-bond partners for either Y28' or D30', which instead are exposed to solvent; however another H-bond network stabilizes the P-loop-S6 linker (L panel 2).

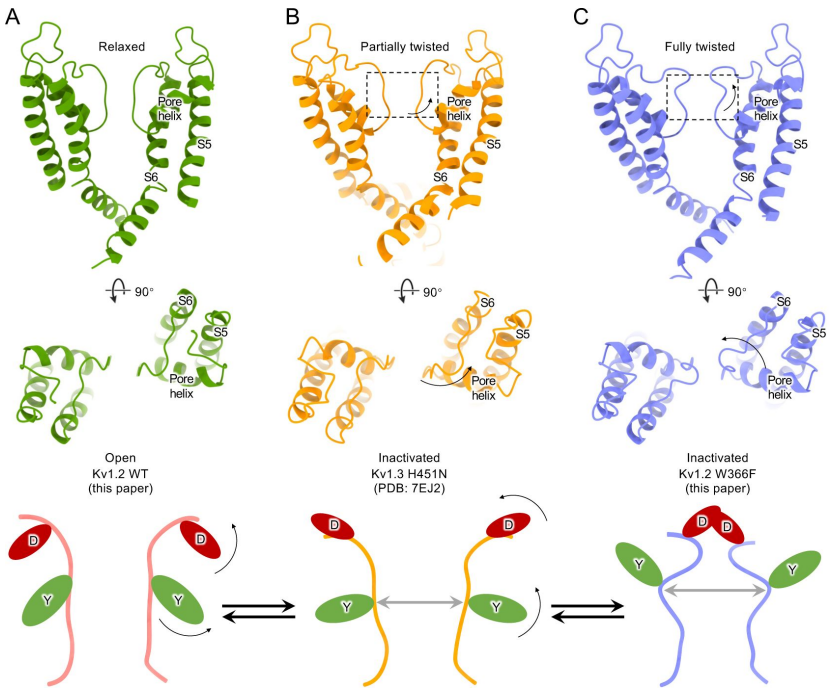

Figure 6 - figure supplement 2.

Summary of conformational changes in Kv channel inactivation. Upper panels: (A) Kv1.2 WT pore domain (PD) in green (B) Kv1.3 H451N PD in orange and (C) Kv1.2 W366F PD in orchid represent the relaxed, partially twisted and fully twisted P-loop respectively. Lower panels: cartoon illustration of (A) relaxed, (B) partially twisted and (C) fully twisted selectivity filter P-loop of Kv channels. D30′ and Y28′ residue side chains are shown as red and green ovals.

References

1. Banerjee A., Lee A., Campbell E., Mackinnon R (2013) **Structure of a pore-blocking toxin in complex with a eukaryotic voltage-dependent K(+) channel** *Elife* **2** https://doi.org/10.7554/eLife.00594

2. Bassetto C. A., Carvalho-de-Souza J. L., Bezanilla F (2021) **Molecular basis for functional connectivity between the voltage sensor and the selectivity filter gate in Shaker K(+) channels** *Elife* **10** https://doi.org/10.7554/eLife.63077

3. Conti L., Renhorn J., Gabrielsson A., Turesson F., Liin S. I., Lindahl E., Elinder F (2016) **Reciprocal voltage sensor-to-pore coupling leads to potassium channel C-type inactivation** *Sci Rep* **6** https://doi.org/10.1038/srep27562

4. Cuello L. G., Cortes D. M., Perozo E (2017) **The gating cycle of a K(+) channel at atomic resolution** *Elife* **6** https://doi.org/10.7554/eLife.28032

5. Doyle D. A., Morais Cabral J., Pfuetzner R. A., Kuo A., Gulbis J. M., Cohen S. L., Chait B. T., MacKinnon R (1998) **The structure of the potassium channel: molecular basis of K+ conduction and selectivity** *Science* **280**:69–77 https://doi.org/10.1126/science.280.5360.69

6. Emsley P., Lohkamp B., Scott W. G., Cowtan K (2010) **Features and development of Coot** *Acta Crystallogr D Biol Crystallogr* **66**:486–501 https://doi.org/10.1107/S0907444910007493

7. Gasparini S., Danse J. M., Lecoq A., Pinkasfeld S., Zinn-Justin S., Young L. C., de Medeiros C. C., Rowan E. G., Harvey A. L., Menez A. (1998) **Delineation of the functional site of alpha-dendrotoxin. The functional topographies of dendrotoxins are different but share a conserved core with those of other Kv1 potassium channel-blocking toxins** *J Biol Chem* **273** https://doi.org/10.1074/jbc.273.39.25393

8. Goddard T. D., Huang C. C., Meng E. C., Pettersen E. F., Couch G. S., Morris J. H., Ferrin T. E (2018) **UCSF ChimeraX: Meeting modern challenges in visualization and analysis** *Protein Sci* **27**:14–25 https://doi.org/10.1002/pro.3235

9. Gulbis J. M., Mann S., MacKinnon R (1999) **Structure of a voltage-dependent K+ channel beta subunit** *Cell* **97**:943–952 https://doi.org/10.1016/s0092-8674(00)80805-3

10. Gulbis J. M., Zhou M., Mann S., MacKinnon R (2000) **Structure of the cytoplasmic beta subunit-T1 assembly of voltage-dependent K+ channels** *Science* **289**:123–127 https://doi.org/10.1126/science.289.5476.123

11. Harvey A. L., Rowan E. G., Vatanpour H., Engstrom A., Westerlund B., Karlsson E (1997) **Changes to biological activity following acetylation of dendrotoxin I from Dendroaspis polylepis (black mamba)** *Toxicon* **35**:1263–1273 https://doi.org/10.1016/s0041-0101(97)00016-0

12. Heginbotham L., Lu Z., Abramson T., MacKinnon R (1994) **Mutations in the K+ channel signature sequence** *Biophys J* **66**:1061–1067 https://doi.org/10.1016/S0006-3495(94)80887-2

13. Hodgkin A. L., Huxley A. F (1952) **The components of membrane conductance in the giant axon of Loligo** *J Physiol* **116**:473–496 https://doi.org/10.1113/jphysiol.1952.sp004718

14. Hoshi T., Zagotta W. N., Aldrich R. W (1991) **Two types of inactivation in Shaker K+ channels: effects of alterations in the carboxy-terminal region** *Neuron* **7**:547–556 https://doi.org/10.1016/0896-6273(91)90367-9

15. Ishida I. G., Rangel-Yescas G. E., Carrasco-Zanini J., Islas L. D (2015) **Voltage-dependent gating and gating charge measurements in the Kv1.2 potassium channel** *J Gen Physiol* **145**:345–358 https://doi.org/10.1085/jgp.201411300

16. Islas L. D (2016) **Functional diversity of potassium channel voltage-sensing domains** *Channels (Austin* **10**:202–213 https://doi.org/10.1080/19336950.2016.1141842

17. Iverson L. E., Tanouye M. A., Lester H. A., Davidson N., Rudy B (1988) **A-type potassium channels expressed from Shaker locus cDNA** *Proc Natl Acad Sci U S A* **85**:5723–5727 https://doi.org/10.1073/pnas.85.15.5723

18. Jensen M. O., Jogini V., Borhani D. W., Leffler A. E., Dror R. O., Shaw D. E (2012) **Mechanism of voltage gating in potassium channels** *Science* **336**:229–233 https://doi.org/10.1126/science.1216533

19. Karbat I. *et al.* (2019) **Pore-modulating toxins exploit inherent slow inactivation to block K(+) channels** *Proc Natl Acad Sci U S A* **116**:18700–18709 https://doi.org/10.1073/pnas.1908903116

20. Kondo H. X., Yoshida N., Shirota M., Kinoshita K (2018) **Molecular Mechanism of Depolarization-Dependent Inactivation in W366F Mutant of Kv1.2** *J Phys Chem B* **122**:10825–10833 https://doi.org/10.1021/acs.jpcb.8b09446

21. Korn S. J., Ikeda S. R (1995) **Permeation selectivity by competition in a delayed rectifier potassium channel** *Science* **269**:410–412 https://doi.org/10.1126/science.7618108

22. Lee C. H., MacKinnon R (2017) **Structures of the Human HCN1 Hyperpolarization-Activated Channel** *Cell* **168**:111–120 https://doi.org/10.1016/j.cell.2016.12.023

23. Lee S. Y., MacKinnon R (2004) **A membrane-access mechanism of ion channel inhibition by voltage sensor toxins from spider venom** *Nature* **430**:232–235 https://doi.org/10.1038/nature02632

24. Levy D. I., Deutsch C (1996) **Recovery from C-type inactivation is modulated by extracellular potassium** *Biophys J* **70**:798–805 https://doi.org/10.1016/S0006-3495(96)79619-4

25. Li J., Ostmeyer J., Cuello L. G., Perozo E., Roux B (2018) **Rapid constriction of the selectivity filter underlies C-type inactivation in the KcsA potassium channel** *J Gen Physiol* **150**:1408–1420 https://doi.org/10.1085/jgp.201812082

26. Li J., Shen R., Reddy B., Perozo E., Roux B (2021) **Mechanism of C-type inactivation in the hERG potassium channel** *Sci Adv* **7** https://doi.org/10.1126/sciadv.abd6203

27. Li J., Shen R., Rohaim A., Mendoza Uriarte R., Fajer M., Perozo E., Roux B (2021) **Computational study of non-conductive selectivity filter conformations and C-type inactivation in a voltage-dependent potassium channel** *J Gen Physiol* **153** https://doi.org/10.1085/jgp.202112875

28. Liebschner D. *et al.* (2019) **Macromolecular structure determination using X-rays, neutrons and electrons: recent developments in Phenix** *Acta Crystallogr D Struct Biol* **75**:861–877 https://doi.org/10.1107/S2059798319011471

29. Liu S., Zhao Y., Dong H., Xiao L., Zhang Y., Yang Y., Ong S. T., Chandy K. G., Zhang L., Tian C (2021) **Structures of wild-type and H451N mutant human lymphocyte potassium channel KV1.3** *Cell Discov* **7** https://doi.org/10.1038/s41421-021-00269-y

30. Lolicato M., Natale A. M., Abderemane-Ali F., Crottes D., Capponi S., Duman R., Wagner A., Rosenberg J. M., Grabe M., Minor D. L. (2020) **K(2P) channel C-type gating involves asymmetric selectivity filter order-disorder transitions** *Sci Adv* **6** https://doi.org/10.1126/sciadv.abc9174

31. Long S. B., Campbell E. B., Mackinnon R (2005) **Crystal structure of a mammalian voltage-dependent Shaker family K+ channel** *Science* **309**:897–903 https://doi.org/10.1126/science.1116269

32. Long S. B., Tao X., Campbell E. B., MacKinnon R (2007) **Atomic structure of a voltage-dependent K+ channel in a lipid membrane-like environment** *Nature* **450**:376–382 https://doi.org/10.1038/nature06265

33. Matamoros M., Ng X. W., Brettmann J. B., Piston D. W., Nichols C. G (2023) **Conformational plasticity of NaK2K and TREK2 potassium channel selectivity filters** *Nat Commun* **14** https://doi.org/10.1038/s41467-022-35756-7

34. Matthies D., Bae C., Toombes G. E., Fox T., Bartesaghi A., Subramaniam S., Swartz K. J (2018) **Single-particle cryo-EM structure of a voltage-activated potassium channel in lipid nanodiscs** *Elife* **7** https://doi.org/10.7554/eLife.37558

35. Melishchuk A., Loboda A., Armstrong C. M (1998) **Loss of shaker K channel conductance in 0 K+ solutions: role of the voltage sensor** *Biophys J* **75**:1828–1835 https://doi.org/10.1016/S0006-3495(98)77624-6

36. Morais-Cabral J. H., Zhou Y., MacKinnon R (2001) **Energetic optimization of ion conduction rate by the K+ selectivity filter** *Nature* **414**:37–42 https://doi.org/10.1038/35102000

37. Murshudov G. N., Skubak P., Lebedev A. A., Pannu N. S., Steiner R. A., Nicholls R. A., Winn M. D., Long F., Vagin A. A (2011) **REFMAC5 for the refinement of macromolecular crystal structures** *Acta Crystallogr D Biol Crystallogr* **67**:355–367 https://doi.org/10.1107/S0907444911001314

38. Noskov S. Y., Roux B (2006) **Ion selectivity in potassium channels** *Biophys Chem* **124**:279–291 https://doi.org/10.1016/j.bpc.2006.05.033

39. Papazian D. M., Schwarz T. L., Tempel B. L., Jan Y. N., Jan L. Y (1987) **Cloning of genomic and complementary DNA from Shaker, a putative potassium channel gene from Drosophila** *Science* **237**:749–753 https://doi.org/10.1126/science.2441470

40. Perozo E., MacKinnon R., Bezanilla F., Stefani E (1993) **Gating currents from a nonconducting mutant reveal open-closed conformations in Shaker K+ channels** *Neuron* **11**:353–358 https://doi.org/10.1016/0896-6273(93)90190-3

41. Pettersen E. F., Goddard T. D., Huang C. C., Couch G. S., Greenblatt D. M., Meng E. C., Ferrin T. E (2004) **UCSF Chimera--a visualization system for exploratory research and analysis** *J Comput Chem* **25**:1605–1612 https://doi.org/10.1002/jcc.20084

42. Pless S. A., Galpin J. D., Niciforovic A. P., Kurata H. T., Ahern C. A (2013) **Hydrogen bonds as molecular timers for slow inactivation in voltage-gated potassium channels** *Elife* **2** https://doi.org/10.7554/eLife.01289

43. Reddi R., Matulef K., Riederer E. A., Whorton M. R., Valiyaveetil F. I (2022) **Structural basis for C-type inactivation in a Shaker family voltage-gated K(+) channel** *Sci Adv* **8** https://doi.org/10.1126/sciadv.abm8804

44. Rettig J., Heinemann S. H., Wunder F., Lorra C., Parcej D. N., Dolly J. O., Pongs O (1994) **Inactivation properties of voltage-gated K+ channels altered by presence of beta-subunit** *Nature* **369**:289–294 https://doi.org/10.1038/369289a0

45. Rosenthal J. J., Bezanilla F (2002) **A comparison of propagated action potentials from tropical and temperate squid axons: different durations and conduction velocities correlate with ionic conductance levels** *J Exp Biol* **205**:1819–1830 https://doi.org/10.1242/jeb.205.12.1819

46. Roux B (2005) **Ion conduction and selectivity in K(+) channels** *Annu Rev Biophys Biomol Struct* **34**:153–171 https://doi.org/10.1146/annurev.biophys.34.040204.144655

47. Sauer D. B., Zeng W., Raghunathan S., Jiang Y (2011) **Protein interactions central to stabilizing the K+ channel selectivity filter in a four-sited configuration for selective K+ permeation** *Proc Natl Acad Sci U S A* **108**:16634–16639 https://doi.org/10.1073/pnas.1111688108

48. Schorb M., Haberbosch I., Hagen W. J. H., Schwab Y., Mastronarde D. N (2019) **Software tools for automated transmission electron microscopy** *Nat Methods* **16**:471–477 https://doi.org/10.1038/s41592-019-0396-9

49. Selvakumar P. *et al.* (2022) **Structures of the T cell potassium channel Kv1.3 with immunoglobulin modulators** *Nat Commun* **13** https://doi.org/10.1038/s41467-022-31285-5

50. Shealy R. T., Murphy A. D., Ramarathnam R., Jakobsson E., Subramaniam S. (2003) **Sequence-function analysis of the K+-selective family of ion channels using a comprehensive alignment and the KcsA channel structure** *Biophys J* **84** https://doi.org/10.1016/S0006-3495(03)70020-4

51. Shi N., Ye S., Alam A., Chen L., Jiang Y (2006) **Atomic structure of a Na+- and K+- conducting channel** *Nature* **440**:570–574 https://doi.org/10.1038/nature04508

52. Skarzynski T (1992) **Crystal structure of alpha-dendrotoxin from the green mamba venom and its comparison with the structure of bovine pancreatic trypsin inhibitor** *J Mol Biol* **224**:671–683 https://doi.org/10.1016/0022-2836(92)90552-u

53. Starkus J. G., Kuschel L., Rayner M. D., Heinemann S. H (1997) **Ion conduction through C- type inactivated Shaker channels** *J Gen Physiol* **110**:539–550 https://doi.org/10.1085/jgp.110.5.539

54. Starkus J. G., Kuschel L., Rayner M. D., Heinemann S. H (1998) **Macroscopic Na+ currents in the "Nonconducting" Shaker potassium channel mutant W434F** *J Gen Physiol* **112**:85–93 https://doi.org/10.1085/jgp.112.1.85

55. Suarez-Delgado E., Rangel-Sandin T. G., Ishida I. G., Rangel-Yescas G. E., Rosenbaum T., Islas L. D (2020) **KV1.2 channels inactivate through a mechanism similar to C-type inactivation** *J Gen Physiol* **152** https://doi.org/10.1085/jgp.201912499

56. Tan X. F., Bae C., Stix R., Fernandez-Marino A. I., Huffer K., Chang T. H., Jiang J., Faraldo- Gomez J. D., Swartz K. J (2022) **Structure of the Shaker Kv channel and mechanism of slow C-type inactivation** *Sci Adv* **8** https://doi.org/10.1126/sciadv.abm7814

57. Tao X., Lee A., Limapichat W., Dougherty D. A., MacKinnon R (2010) **A gating charge transfer center in voltage sensors** *Science* **328**:67–73 https://doi.org/10.1126/science.1185954

58. Tao X., MacKinnon R (2008) **Functional analysis of Kv1.2 and paddle chimera Kv channels in planar lipid bilayers** *J Mol Biol* **382**:24–33 https://doi.org/10.1016/j.jmb.2008.06.085

59. Tyagi A. *et al.* (2022) **Rearrangement of a unique Kv1.3 selectivity filter conformation upon binding of a drug** *Proc Natl Acad Sci U S A* **119** https://doi.org/10.1073/pnas.2113536119

60. Wang J. M., Roh S. H., Kim S., Lee C. W., Kim J. I., Swartz K. J (2004) **Molecular surface of tarantula toxins interacting with voltage sensors in K(v) channels** *J Gen Physiol* **123**:455–467 https://doi.org/10.1085/jgp.200309005

61. Wang S., Lee S. J., Maksaev G., Fang X., Zuo C., Nichols C. G (2019) **Potassium channel selectivity filter dynamics revealed by single-molecule FRET** *Nat Chem Biol* **15**:377–383 https://doi.org/10.1038/s41589-019-0240-7

62. Wu X., Gupta K., Swartz K. J (2022) **Mutations within the selectivity filter reveal that Kv1 channels have distinct propensities to slow inactivate** *J Gen Physiol* **154** https://doi.org/10.1085/jgp.202213222

63. Yang Y., Yan Y., Sigworth F. J (1997) **How does the W434F mutation block current in Shaker potassium channels?** *J Gen Physiol* **109**:779–789 https://doi.org/10.1085/jgp.109.6.779

64. Zhang K (2016) **Gctf: Real-time CTF determination and correction** *J Struct Biol* **193**:1–12 https://doi.org/10.1016/j.jsb.2015.11.003

65. Zhang K., Julius D., Cheng Y (2021) **Structural snapshots of TRPV1 reveal mechanism of polymodal functionality** *Cell* **184**:5138–5150 https://doi.org/10.1016/j.cell.2021.08.012

66. Zheng S. Q., Palovcak E., Armache J. P., Verba K. A., Cheng Y., Agard D. A (2017) **MotionCor2: anisotropic correction of beam-induced motion for improved cryo-electron microscopy** *Nat Methods* **14**:331–332 https://doi.org/10.1038/nmeth.4193

67. Zhou Y., Morais-Cabral J. H., Kaufman A., MacKinnon R (2001) **Chemistry of ion coordination and hydration revealed by a K+ channel-Fab complex at 2.0 A resolution** *Nature* **414**:43–48 https://doi.org/10.1038/35102009

Article and author information

Yangyu Wu

Department of Cellular and Molecular Physiology, Yale University School of Medicine, New Haven, Connecticut USA

Yangyang Yan
Department of Cellular and Molecular Physiology, Yale University School of Medicine, New Haven, Connecticut USA

Youshan Yang
Department of Cellular and Molecular Physiology, Yale University School of Medicine, New Haven, Connecticut USA

Shumin Bian
Department of Cellular and Molecular Physiology, Yale University School of Medicine, New Haven, Connecticut USA

Alberto Rivetta
Department of Cellular and Molecular Physiology, Yale University School of Medicine, New Haven, Connecticut USA

Ken Allen
Department of Cellular and Molecular Physiology, Yale University School of Medicine, New Haven, Connecticut USA

Fred J. Sigworth
Department of Cellular and Molecular Physiology, Yale University School of Medicine, New Haven, Connecticut USA
For correspondence: fred.sigworth@yale.edu

Copyright

Editors

Reviewing Editor
Leon Islas
Universidad Nacional Autónoma de México, México City, Mexico

Senior Editor
Kenton Swartz
National Institute of Neurological Disorders and Stroke, Bethesda, United States of America

Reviewer #1 (Public Review):

In this manuscript by Wu et al., the authors present the high resolution cryoEM structures of the WT Kv1.2 voltage-gated potassium channel. Along with this structure the authors have solved several structures of mutants or experimental conditions relevant to the slow inactivation process that these channels undergo and which is not yet completely understood.

One of the main findings is the determination of the structure of a mutant (W366F) that is thought to correspond to the slow inactivated state. These experiments confirm results in

similar mutants in different channels from Kv1.2 that indicate that inactivation is associated with an enlarged selectivity filter.

Another interesting structure is the complex of Kv1.2 with the pore blocking toxin Dendrotoxin 1. The results shown in the revised version indicate that the mechanism of block is similar to that of related blocking-toxins, in which a lysine residue penetrates in the pore. Surprisingly, in these new structures, the bound toxin results in a pore with empty external potassium binding sites.

The quality of the structural data presented in this revised manuscript is very high and allows for unambiguous assignment of side chains. The conclusions are supported by the data. This is an important contribution that should further our understanding of voltage-dependent potassium channel gating. In the revised version, the authors have addressed my previous specific comments, which are appended below.

(1) In the main text's reference to Figure 2d residues W18' and S22' are mentioned but are not labeled in the insets.

(2) On page 8 there is a discussion of how the two remaining K+ ions in binding sites S3 and S4 prevent permeation K+ in molecular dynamics. However, in Shaker, inactivated W434F channels can sporadically allow K+ permeation with normal single-channel conductance but very reduced open times and open probability at not very high voltages.

(3) The structures of WT in the absence of K+ shows a narrower selectivity filter, however Figure 4 does not convey this finding. In fact, the structure in Figure 4B is constructed in such an angle that it looks as if the carbonyl distances are increased, perhaps this should be fixed. Also, it is not clear how the distances between carbonyls given in the text on page 12 are measured. Is it between adjacent or kitty-corner subunits?

(4) It would be really interesting to know the authors opinion on the driving forces behind slow inactivation. For example, potassium flux seems to be necessary for channels to inactivate, which might indicate a local conformational change is the trigger for the main twisting events proposed here.

https://doi.org/10.7554/eLife.89459.2.sa2

Reviewer #2 (Public Review):

Cryo_EM structures of the Kv1.2 channel in the open, inactivated, toxin complex and in Na+ are reported. The structures of the open and inactivated channels are merely confirmatory of previous reports. The structures of the dendrotoxin bound Kv1.2 and the channel in Na+ are new findings that will of interest to the general channel community.

Review of the resubmission:

I thank the authors for making the changes in their manuscript as suggested in the previous review. The changes in the figures and the additions to the text do improve the manuscript. The new findings from a further analysis of the toxin channel complex are welcome information on the mode of the binding of dendrotoxin.

A few minor concerns:
(1) Line 93-96, 352: I am not sure as to what is it the authors are referring to when they say NaK2P. It is either NaK or NaK2K. I don't think that it has been shown in the reference suggested that either of these channels change conformation based on the K+ concentration. Please check if there is a mistake and that the Nichols et. al. reference is what is being referred to.

(2) Line 365: In the study by Cabral et. al., Rb+ ions were observed by crystallography in the S1, S3 and S4 site, not the S2 site. Please correct.

https://doi.org/10.7554/eLife.89459.2.sa1

Reviewer #3 (Public Review):

Wu et al. present cryo-EM structures of the potassium channel Kv1.2 in open, C-type inactivated, toxin-blocked and presumably sodium-bound states at 3.2 Å, 2.5 Å, 2.8 Å, and 2.9 Å. The work builds on a large body of structural work on Kv1.2 and related voltage-gated potassium channels. The manuscript presents a plethora of structural work, and the authors are commended on the breadth of the studies. The structural studies are well-executed. Although the findings are mostly confirmatory, they do add to the body of work on this and related channels. Notably, the authors present structures of DTx-bound Kv1.2 and of Kv1.2 in a low concentration of potassium (which may contain sodium ions bound within the selectivity filter). These two structures add considerable new information. The DTx structure has been markedly improved in the revised version and the authors arrive at well-founded conclusions regarding its mechanism of block. Regarding the Na+ structure, the authors claim that the structure with sodium has "zero" potassium - I caution them to make this claim. It is likely that some K+ persists in their sample and that some of the density in the "zero potassium" structure may be due to K+ rather than Na+. This can be clarified by revisions to the text and discussion. I do not think that any additional experiments are needed. Overall, the manuscript is well-written, a nice addition to the field, and a crowning achievement for the Sigworth lab.

Most of this reviewer's initial comments have been addressed in the revised manuscript. Some comments remain that could be addressed by revisions of the text.

Specific comments on the revised version:
Quotations indicate text in the manuscript.
(1) "While the VSD helices in Kv1.2s and the inactivated Kv1.2s-W17'F superimpose very well at the top (including the S4-S5 interface described above), there is a general twist of the helix bundle that yields an overall rotation of about 3o at the bottom of the VSD."

Comment: This seemed a bit confusing. I assume the authors aligned the complete structures - the differences they indicate seem to be slight VSD repositioning relative to the pore rather than differences between the VSD conformations themselves. The authors may wish to clarify. As they point out in the subsequent paragraph, the VSDs are known to be loosely associated with the pore.

(2) Comment: The modeling of DTx into the density is a major improvement in the revision. Figure 3 displays some interactions between the toxin and Kv1.2 - additional side views of the toxin and the channel might allow the reader to appreciate the interactions more fully. The overall fit of the toxin structure into the density is somewhat difficult to assess from the figure. (The authors might consider using ChimeraX to display density and model in this figure.)

(3) "We obtained the structure of Kv1.2s in a zero K+ solution, with all potassium replaced with sodium, and were surprised to find that it is little changed from the K+ bound structure, with an essentially identical selectivity filter conformation (Figure 4B and Figure 4-figure supplement 1)."

Comment: It should be noted in the manuscript that K+ and Na+ ions cannot be distinguished by the cryo-EM studies - the densities are indistinguishable. The authors are inferring that the observed density corresponds to Na+ because the protein was exchanged from K+ into Na+

on a gel filtration (SEC) column. It is likely that a small amount of K+ remains in the protein sample following SEC. I caution the authors to claim that there is zero K+ in solution without measuring the K+ content of the protein sample. Additionally, it should be considered that K+ may be present in the blotting paper used for cryo-EM grid preparation (our laboratory has noted, for example, a substantial amount of Ca2+ in blotting paper). The affinity of Kv1.2 for K+ has not been determined, to my knowledge - the authors note in the Discussion that the Shaker channel has "tight" binding for K+. It seems possible that some portion of the density in the selectivity filter could be due to residual K+. This caveat should be clearly stated in the main text and discussion. More extensive exchange into Na+, such as performing the entire protein purification in NaCl, or by dialysis (as performed for obtaining the structure of KcsA in low K+ by Y. Zhou et al. & Mackinnon 2001), would provide more convincing removal of K+, but I suspect that the Kv1.2 protein would not have sufficient biochemical stability without K+ to endure this treatment. One might argue that reduced biochemical stability in NaCl could be an indication that there was a meaningful amount of K+ in the final sample used for cryo-EM (or in the particles that were selected to yield the final high-resolution structure).

(4) Referring to the structure obtained in NaCl: "The ion occupancy is also similar, and we presume that Kv1.2 is a conducting channel in sodium solution."

Comment: Stating that "Kv1.2 is a conducting channel in sodium solution" and implying that conduction of Na+ is achieved by an analogous distribution of ion binding sites as observed for K+ are strong statements to make - and not justified by the experiments provided. Electrophysiology would be required to demonstrate that the channel conducts sodium in the absence of K+. More complete ionic exchange, better control of the ionic conditions (Na+ vs K+), and affinity measurements for K+ would be needed to determine the distribution of Na+ in the filter (as mentioned above). At minimum, the authors should revise and clarify what the intended meaning of the statement "we presume that Kv1.2 is a conducting channel in sodium solution". As mentioned above, it seems possible/likely that a portion of the density in the filter may be due to K+.

https://doi.org/10.7554/eLife.89459.2.sa0

Author response:

The following is the authors' response to the original reviews.

> ***Public Reviews:***
>
> ***Reviewer #1 (Public Review):***
>
> *In this manuscript by Wu et al., the authors present the high-resolution cryoEM structures of the WT Kv1.2 voltage-gated potassium channel. Along with this structure, the authors have solved several structures of mutants or experimental conditions relevant to the slow inactivation process that these channels undergo and which is not yet completely understood.*
>
> *One of the main findings is the determination of the structure of a mutant (W366F) that is thought to correspond to the slow inactivated state. These experiments confirm results in similar mutants in different channels from Kv1.2 that indicate that inactivation is associated with an enlarged selectivity filter.*
>
> *Another interesting structure is the complex of Kv1.2 with the pore-blocking toxin Dendrotoxin 1. The results show that the mechanism of the block is different from similar*

> *toxins, in which a lysine residue penetrates the pore deep enough to empty most external potassium binding sites.*
>
> *The quality of the structural data presented in this manuscript is very high and allows for the unambiguous assignment of side chains. The conclusions are supported by the data. This is an important contribution that should further our understanding of voltagedependent potassium channel gating. Specific comments are appended below.*
>
> *(1) In the mains text's reference to Figure 2d residues W18' and S22' are mentioned but are not labeled in the insets.*

Now labeled in Fig. 2D

> *(2) On page 8 there is a discussion of how the two remaining K+ ions in binding sites S3 and S4 prevent permeation K+ in molecular dynamics. However, in Shaker, inactivated W434F channels can sporadically allow K+ permeation with normal single-channel conductance but very reduced open times and open probability at not very high voltages.*

Addressed in the Discussion, lines 480-490.

> *(3) The structures of WT in the absence of K+ show a narrower selectivity filter, however, Figure 4 does not convey this finding. In fact, the structure in Figure 4B is constructed at such an angle that it looks as if the carbonyl distances are increased, perhaps this should be fixed. Also, it is not clear how the distances between carbonyls given in the text on page 12 are measured. Is it between adjacent or kitty-corner subunits?*

We decided to remove mention of carbonyl distances, because at our resolutions the atoms are not resolved.

> *(4) It would be really interesting to know the authors' opinions on the driving forces behind slow inactivation. For example, potassium flux seems to be necessary for channels to inactivate, which might indicate a local conformational change is the trigger for the main twisting events proposed here.*

We cite Sauer et al. (2011) for the idea that the intact selectivity filter is a strained conformation, and its relaxation yields the wide vestibule seen in NaK2K and Kv channels. Lines 434-439.

> ***Reviewer #2 (Public Review):***
>
> *There are four Kv1.2 channel structures reported: the open state, the C-type inactivated state, a dendrotoxin-bound state, and a structure in Na+.*

A high-resolution crystal structure of the open state for a chimeric Kv1.2 channel was reported in 2007 and there is no new information provided by the cryoEM structure reported in this study.

> *The cryo-EM structure of the C-type inactivated state of the Kv1.2 channel was determined for a channel with the W to F substitution in the pore helix. A cryo-EM structure of the Shaker channel and a crystal structure of a chimeric Kv1.2 channel with an equivalent W to F mutation were reported in 2022. Cryo-EM structures of the C-type inactivated Kv1.3 channel are also available. All these previous structures have provided a relatively consistent structural view of the C-type inactivated state and there is no significant new information that is provided by the structure reported in this study.*

> *A structure of the Kv1.2 channel blocked by dendrotoxin is reported. A crystal structure of charybdotoxin and the chimeric Kv1.2 channel was reported in 2013. Density for dendrotoxin could not be clearly resolved due to symmetry issues and so the definitive information from the structure is that dendrotoxin binds, similarly to charybdotoxin, at the mouth of the pore. A potential new finding is that there is a deeper penetration of the blocking Lys residue in dendrotoxin compared to charybdotoxin. It will however be necessary to use approaches to break the symmetry and resolve the electron density for the dendrotoxin molecule to support this claim and to make this structure significant.*

We have now succeeded in breaking the symmetry and present in Fig. 3 a C1 structure of the toxin-channel complex. In the improved map we now see that our previous conclusion was wrong: the penetration of Lys5 cannot be much deeper than that seen in CTx and ShK structures. However for some reason the pattern of ion-site occupancies in the blocked state is different in this structure than in the others. Fig. 3, Fig. 4E; text lines 559-568.

> *The final structure reported is the structure of the Kv1.2 channel in K+ free conditions and with Na+ present. The structure of the KcsA channel by the MacKinnon group in 2001 showed a constricted filter and since then it has been falsely assumed by the K channel community that the lowering of K concentration leads to a construction of the selectivity filter. There have been structural studies on the MthK and the NaK2K channels showing a lack of constriction in the selectivity filter in the absence of K+. These results have been generally ignored and the misconception of filter constriction/collapse in the absence of K+ still persists. The structure of the Kv1.2 channel in Na+ provided a clear example that loss of K+ does not necessarily lead to filter constriction.*

We are grateful to the reviewer for pointing out this serious omission. We now cite other work including from the Y. Jiang and C. Nichols labs showing examples of outer pore expansion and destabilization. Page p. 4, lines 90-104; lines 421-439.

> *The structure in Na+ is significant while the other structures are either merely reproductions of previous reports or are not resolved well enough to make any substantial claims.*

We now state more clearly the confirmatory nature of our Kv1.2 open structure (lines 71-74) and the similarities of the inactivated-channel structures (lines 193196).

> ***Reviewer #3 (Public Review):***
>
> *Wu et al. present cryo-EM structures of the potassium channel Kv1.2 in open, C-type inactivated, toxin-blocked and presumably sodium-bound states at 3.2 Å, 2.5 Å, 2.8 Å, and 2.9 Å. The work builds on a large body of structural work on Kv1.2 and related voltage-gated potassium channels. The manuscript presents a large quantity of structural work on the Kv1.2 channel, and the authors should be commended on the breadth of the studies. The structural studies seem well-executed (this is hard to fully evaluate because the current manuscript is missing a data collection and refinement statistics table). The findings are mostly confirmatory, but they do add to the body of work on this and related channels. Notably, the authors present structures of DTXbound Kv1.2 and of Kv1.2 in a low concentration of potassium (with presumably sodium ions bound within the selectivity filter). These two structures add new information, but the studies seem somewhat underdeveloped - they would be strengthened by accompanying functional studies and further structural analyses. Overall, the manuscript is well-written and a nice addition to the field.*

The data collection and refinement table has been added (Fig. 4 supplement 3.)

We agree and regret the lack of functional studies. We have not been able to carry them out because work in our laboratory is winding down and the lab soon will be closing.

> ***Recommendations for the authors:***
>
> ***Reviewer #2 (Recommendations For The Authors):***
>
> *(1) It is not obvious from the data shown how well the side chain positions in the inactivated state are defined by the electron density. These figures should be redone. Maybe the use of stereo would be useful. This will be particularly useful for the reader to decide if the small changes in, for example, the positioning of the carbonyl oxygens are believable.*

Figure 2 – figure supplement 4 shows the stereo views.

> *(2) The authors note the changes observed (though small) in the VSD which were not observed in other structures. The relevance of this observation is not described. Do these changes arise due to the different environments of detergents versus nanodisc etc. in the different structures?*

We've now inserted a note about variety of environments and how this might be a cause of the difference: lines 280-285.

> *Are there changes in the pore-VSD interface in the inactivated and the open channel structures and if yes, then do mutations at these residues affect inactivation?*

There is surprisingly little movement at the S4-S5 interface residues identified by Bassetto et al. (2022) as having effects on inactivation. Lines 262-267.

> *(3) For the structures in Na+, it is important to provide analytical data showing the biochemical behavior of the channel. This is also true for the wild type and the W to F mutant channel. Size exclusion profiles should be included.*

The SEC profile (noisy, but showing a clear peak) of the channel in Na+ is now shown in Fig. 4 supplement 1. Low expression of the W366F mutant produced even worse SEC results, but we include a representative micrograph of W366F in Na+ to show the monodispersed protein prep. In Figure 5 – figure supplement 1.

> ***Reviewer #3 (Recommendations For The Authors):***
>
> *Portions of text from the manuscript are indicated by quotations.*
>
> *Introduction: "One goal of the current study was to examine the structure of the native Kv1.2 channel."*
>
> *Comment, minor points: The authors refer to the Kv1.2 construct used for the structural studies as "native Kv1.2". I found this somewhat confusing because the word "native" suggests derived from a native source. The phrasing above also gives the impression that the structure by Wu et al is the first structure of Kv1.2. The Kv1.2 construct is essentially identical to the one used by Long et al in 2005 to determine the initial structure of Kv1.2 (PDB 2A79). The authors discuss a subsequent paddle-chimera Kv1.2-2.1 structure from 2007 (PDB 2R9R) in the introduction, but it would be prudent to mention the 2005 one of Kv1.2 as well. The open structure determined by Wu et al. is an improvement on the 2A79 structure in that the 2A79 structure was modeled as a poly-alanine model within the voltage sensor domain. Nevertheless, the Kv1.2-2.1 structure (2R9R) is highly similar to*

> *the 2A79 structure of Kv1.2. The 2007 structure indicated that Kv1.2-2.1 recapitulates structural features of Kv1.2. It is therefore not surprising that the open structure presented here is highly similar to that of both PDB 2A79 (Kv1.2) and PDB 2R9R (Kv1.2-2.1).*

We failed to point out the high quality of the original Long et al. 2005 structure and its comparisons with the chimeric structure in Long et al. 2007. We now have tried to correct this: lines 70-74.

> *Comment: The cryo-EM analyses suggest that a large percentage (most?) of the particles are missing the beta subunit. This should be commented on somewhere.*

Now noted on lines 120-132, we pooled particles with and without beta subunits.

> *Regarding ions in the selectivity filter, one-dimensional plots of the density would strengthen the analysis.*

Now included in Fig. 4.

> *Also, one should mention caveats associated with identifying ions in cryo-EM maps and the added difficulty/uncertainty when the density is located along a symmetry axis (C4 axis, due to the possible build-up of noise). C1 reconstructions, showing density within the filter, if possible, would strengthen the analyses.*

You are correct. However local resolution is highest in the selectivity filter region. So I think that since the CTF-based filtering is constant over all the structure I think the SNR will be good on axis.

> *Comment: The section on channel inactivation could be simplified by stating that the structure is highly similar to W17'F structures of other Kv channels. (And then discussing possible differences).*

We now note, “overall conformational difference is identical…” p. 7, lines 193-196.

> *"Salt bridges involving the S4 Arg and Lys residues are shifted slightly (Figure 2-figure supplement 3A-D). Arg300 (R3) is in close proximity to Glu226 on the S2 helix for the open channel, while R3 is closer to Glu183 in the S2 helix. The Glu226 side chain adopts a visible interaction with R4 in the inactivated state."*
>
> *Comment: The density for these acidic amino acids seems weak, especially in the inactivated state. It seems like a stretch to make much of their possible conformational changes.*

We’ve included stereo pairs in Fig. 2 – figure supplement 4.

> *"By adding 100 nM α-DTx to detergent solubilized Kv1.2 protein we obtained a cryo-EM structure at 2.8 Å resolution of the complex."*
>
> *Comment: 100 nm. might be lower than the Kv concentration. The current methods are ambiguous on the concentration of Kv channel used for the DTx sample. From the methods, it seems possible that 100 nM DTX is a sub-stoichiometric amount relative to the channel. Regardless, the cryo-EM data seems to suggest that a large percentage of particles do not have DTx bound. This surely complicates the interpretation of density within the filter (which has partly been ascribed to a lysine side chain from DTx).*

The reviewer correctly points a potentially serious problem. It turns out that the 100nM figure we quoted was incorrect, and the actual concentration of toxin, >400 nM, was substantially greater than the protein concentration. This is confirmed by the small fraction (<1%) of 3D class particles that do not show the toxin density (lines 303-306).

> *Comment: The methods on atomic structure building/refinement (Protein model building, refinement, and structural analysis) are sparse. A table is needed showing data collection and refinement statistics for each of the structures. This data should also provide average B factors for the ions in the filter. An example can be found in PMID 36224384.*

Data collection and statistics are now in Fig. 4 – figure supplement 3.

> *"In the selectivity filter of the toxin-bound channel (Figure 3E) a continuous density is seen to extend downward from the external site IS0 through to the boundary between IS1 and IS2. This density is well modeled by an extended Lys side chain from the bound toxin, with the terminal amine coordinated by the carbonyls of G27".*
>
> *Comment: While there seems to be extra density in site IS0 from the figures, the density ascribed to lysine in the filter doesn't seem that distinct from those of ions in the open structure. 1-dimensional density plots and some degree of caution may be prudent. Could there, for example, be a mixture of toxin-bound and free channels in the dataset?*
>
> *Could the lysine penetrate to different depths? If the toxin binds with nM affinity, why are any channels missing the toxin? Have the authors modeled an atomic structure of the entire toxin bound to the channel to evaluate how plausible the proposed binding of the lysine is? Can the toxin be docked onto Kv1.2 with the deep positioning of the lysine and not clash with the extracellular surface of Kv1.2?*

We also were concerned about these issues. We have been able to obtain a C1 reconstruction of the toxin-channel complex. In building the atomic model we found that indeed the Lys5 side chain could not penetrate as far as we had thought, and appears to be coordinated by the first carbonyl pair. Fig. 3; text lines 331-332.

> *"Toxin binding shrinks the distances between opposing carbonyl oxygens in the selectivity filter, forming a narrower tunnel into which the Lys side chain fits (Figure 3F). The second and fourth carbonyl oxygen distances are substantially reduced from 4.7 Å and 4.6 Å in an open state to 3.7 Å and 3.9 Å, respectively (Figure 4E). In a superposition of Kv1.2 open-state and α-DTX-bound P-loop structures, there is also an upward shift of the first three carbonyl groups by 0.7~1.0 Å (Figure 4F). "*
>
> *Comment: I suspect the authors intend to refer to Figure 3F rather than 4. I would be cautious here. The refined positions of the carbonyl oxygens are almost certainly affected by the presence or absence of ions in the atomic model during refinement. The density and the resolution of the map may not be able to distinguish small changes to the positions of the carbonyl oxygens (and these differences/uncertainties are compounded by the C4 symmetry).*
>
> *"On the other hand, the terminal amine of lysine in α-DTX is deeply wedged at the second set of carbonyls, narrowing both IS1 and IS2 while displacing ions from the sites (Figure 3-figure supplement 2A). CTX does not cause narrowing of the selectivity filter or displacements of the carbonyls (Figure 3-figure supplement 2B). "*
>
> *Comment: Again, caution would be prudent here.*

We are very grateful to the reviewer for pointing out these problems. We have removed these statements that are weakly supported at our resolution level.

> *"Shaker channels are able to conduct Na+ in the absence of K+ (Melishchuk et al., 1998)."*
>
> *Comment: How about the Kv1.2 channel? Is Kv1.2 able to conduct Na+ in the absence of K+ ? This would certainly be relevant for interpreting the conformation of the filter and the density ascribed to Na+ for the structure in sodium.*

We agree wholeheartedly, but unfortunately we are no longer capable of doing the measurements as our lab will soon close.

> *"Ion densities are seen in the IS1, IS3, and IS4 ion binding sites, but the selectivity filter shows a general narrowing as would be expected for binding of sodium ions. The second, third, and fourth carbonyl oxygen distances are reduced from 4.7 Å, 4.7 Å, and 4.6 Å in the open state to 4.4 Å, 3.9 Å, and 4.5 Å, respectively. The rest of the channel structure is very little perturbed. "*
>
> *Comment: The density for IS4 seems weak. To me, it looks like IS1 and IS3 are occupied, whereas IS2 and IS4 are much weaker. 1-dimensional density plots would be helpful. I would suggest caution in commenting too strongly on the "general narrowing" since the resolution of the maps, the local density, and the atomic structure refinement would be consistent with coordinate errors of 0.5 Å or more - and would be compounded (~ doubled) by measuring between symmetry-related atoms.*

We present 1D plots in Fig. 4E. We no longer comment on “narrowing”

> *"Finally, the snake toxin a-Dendrotoxin (DTx) studied here is seen to block Kv1.2 by insertion of a lysine residue into the pore."*
>
> *Comment: Discussion (and references) should be given regarding what was known prior to this study on the mode of inhibition by DTx.*

Discussion and references now added, lines 287-301.

> *"On the other hand, a lengthy molecular-dynamics simulation of deactivation in the Kv1.2-2.1..."*
>
> *Comment: I don't think mentioning this personal communication adds to the manuscript.*

Actually the original “personal communication” reference was there because the situation is complicated. The movie S3 accompanying the Jensen et al. paper shows deactivation and dewetting of the channel during a 250 us simulation. In the movie there are ions visible in the selectivity filter for the first 50 us, but after that the SF appears empty. Puzzled by this we contacted Dr. Jensen who explained that the movie was in error, ions remain in the SF throughout the entire 250 us. We now cite Jensen (2012) along with the personal communication.

> *"The difference between the open and inactivated Kv1.2 structures, like the difference in Kv1.2-2.1 (Reddi et al., 2022) and Shaker (Tan et al., 2022) can be imagined as resulting from a two-step process."*
>
> *Comment: Confusing phrasing because the authors mean to compare their structure to inactivated structures of Kv1.2-2.1 and shaker.*

Fixed, lines 220-222.

> *"Molecular dynamics simulations by Tan et al. based on the Shaker-W17'F structure show that IS3 and IS4 are simultaneously occupied by K+ ions in the inactivated state."*
>
> *Comment: I think that the word "show" is too strong. Perhaps "suggest"*

The MD result seems to us to be unequivocal, that most of the time the two sites are occupied by ions.

> *References are needed for the following statements:*
>
> *- "as well as the charge-transfer center phenylalanine"*

Now citing Tao et al. 2010, line 156.

> *- "total gating charge movement in Shaker channels is larger, about 13 elementary charges per channel"*

Now citing the review by Islas, 2015 (line 166-169).

> *"The selectivity filter of potassium channels consists of an array of four copies of the extended loop (the P-loop) formed by a highly conserved sequence, in this case, TTVGYGD. Two residues anchor the outer half of the selectivity filter and are particularly important in inactivation mechanisms (Figure 2B, right panels). Normally, the tyrosine Y28' (Y377 in Kv1.2) is constrained by hydrogen bonds to residues in the pore helix and helix S6 and is key to the conformation of the selectivity filter. The final aspartate of the P-loop, D30' (D379 in Kv1.2) is normally located near the extracellular surface and has a side chain that also participates in H-bonds with W17' (W366 in Kv1.2) on the pore helix."*

Citations added (Pless 2013, Sauer 2011) lines 211-214.

> *- "During normal conduction, ion binding sites in the selectivity filter are usually occupied by K+ and water molecules in alternation."*

Added Morais-Cabral et al. 2001, p. 17, lines 463-465.

https://doi.org/10.7554/eLife.89459.2.sa4